Appendix A Probabilistic Assessment Cases for Alloy 82/182 Dissimilar Metal Welds in Primary System Piping

A.1 Scope of assessment

The probabilistic modeling presented in this appendix explicitly considers two example large-diameter Alloy 82/182 dissimilar metal welds in PWR primary system piping: a reactor vessel outlet nozzle operating at reactor hot-leg temperature and a reactor coolant pump (RCP) suction/discharge nozzle operating at reactor cold-leg temperature. Through sensitivity cases such as for the magnitude of pipe moment loads at the nozzle location, these two cases effectively represent the effects of peening mitigation of all large-diameter butt welds including reactor vessel outlet and inlet nozzles in Westinghouse-designed plants and RCP suction/discharge nozzles in CE- and B&W-designed plants.

Given the relatively large calculated benefit of peening mitigation for these components as presented below, the conclusions regarding appropriate inspection relief following peening may be extended to moderately sized DMWs such as reactor vessel safety injection nozzles in Westinghouse-designed plants and reactor vessel core flood nozzles in B&W-designed plants.

A.2 Probabilistic modeling methodology

The integrated probabilistic modeling framework that is used to study the effect of peening on DM weld PWSCC combines the individual models discussed in Sections A.3 through A.6. Namely, this integrated probabilistic modeling framework is used to predict leakage criterion statistics over the lifetime of the unit, which are discussed in Section A.7. Results generated with this model, using the inputs and uncertainties discussed in Section A.8, are given in Section A.9.

The DM weld probabilistic model described in this appendix applies a framework similar to that of the xLPR probabilistic software tool ([1], [2]), which is currently under development under sponsorship of NRC and EPRI.10 For example:

---

[10] This project, known as xLPR for Extremely Low Probability of Rupture, is developing a fully probabilistic, fracture-mechanics-based computational tool to evaluate the rupture probability of reactor coolant piping. In the xLPR Pilot Study [2] concluded in 2011, the project was focused on evaluating pipe rupture probabilities within Alloy 82/182 dissimilar metal welds located in lines licensed for leak-before-break (LBB) as allowed under General Design Criterion 4, "Environmental and Dynamic Effects Design Bases," of Appendix A, "General Design Criteria for Nuclear Power Plants," to 10 CFR 50.

- Uncertainty propagation is handled by sampling input and parameter values from appropriately selected probability distributions (with appropriately selected bounds) in the main model loop, prior to the time looping structure. It is noted that for simplicity the model discussed in this report does not treat differently epistemic (i.e., due to incomplete knowledge) and aleatory (i.e., due to random variation) uncertainties.
- Event scheduling for a given weld, including operating, mitigation, inspection, and PWSCC initiation times, is developed in the main loop prior to entering the time looping structure.
- If one or more of the predicted PWSCC initiation times, adjusted for differences in stress and temperature, are less than the final operating time and the peening time (if applied), the time looping structure is entered. Each active flaw is allowed to grow until it coalescences with another active flaw, it achieves through-wall crack growth, it is detected and repaired, or it reaches the end of the operation partially through-wall.
- Initiations, leaks, repairs, among other events, are tracked as a function of operating cycle for each Monte Carlo realization and summary statistics are compiled at the end of each Monte Carlo run.

The probabilistic model discussed in this report has the added capability (relative to the xLPR tool) of allowing correlation of selected input parameters during runtime. Specifically, multi-dimensional normal deviates are computed using a covariance matrix Cholesky-decomposition-based approach as discussed in [3]. For a given pair of correlated input parameters, a Pearson product-moment correlation coefficient, which provides a measure of the strength of the linear relationship between two variables, is specified and the pair of correlated random deviates is then used to sample the relevant input parameter distributions. The Pearson coefficient provides a measure of the strength of the linear relationship between two variables where a value of 1 indicates a perfect positive correlation (i.e., a perfect linear correlation with a positive slope), a value of -1 indicates a perfect negative correlation (i.e., a perfect linear correlation with a negative slope), and a value of 0 indicates that there is no linear relationship between the given variables.

It is noted that for convenience of analysis, the probabilistic model described in this report has been designed to simulate up to three distinct DM welds (i.e., welds with different geometries, temperatures, inspection and mitigation schedules, etc.) during a single Monte Carlo run.

In similar fashion to the structure of the xLPR tool, the model is made up of a main loop with an internal time looping structure. Inside the time looping structure, a flaw looping structures are included to account for multiple flaws and their potential interaction. A high level presentation of the main loop of the probabilistic model for a given weld is presented in Figure A-1 and a more detailed presentation of the time looping structure is given in Figure A-2. The remainder of this section provides an end-to-end description of a DM weld Monte Carlo run.

The initial conditions for the run are defined prior to entering the main loop. These initial conditions include all input parameters that remain constant throughout the run, such as the number and length of operating cycles, the frequency of inspections, certain weld geometry attributes, and the times of mitigation.

Following the definition of the initial conditions the main loop is entered. The main loop is cycled for each Monte Carlo realization and is exited once all of the user-specified Monte Carlo realizations have been completed. After exiting the main loop, the program evaluates the results of the run, outputs certain information relevant to the study, and terminates the run.

At the beginning of each Monte Carlo realization, the values of the distributed inputs (detailed in Section A.8) are determined by random sampling. The distributions for each of the distributed inputs are user-defined. The program then calls the load models (detailed in Section A.3) to determine the relevant circumferential or axial loads (including peening loads if peening is scheduled before the end of plant operation).

Once all stresses have been determined from the load model, the program invokes the initiation model (detailed in Section A.4) to predict the initiation times at all potential flaw sites. The flaw initiation times are compared to the "initiation end time": the final operating time or, if peening is scheduled, the peening application time. It is assumed that flaws may not initiate on the component surface after the application of peening. The current Monte Carlo realization is terminated if all of the predicted initiation times exceed the "initiation end time". If not, the initiation model assigns initiation conditions to each flaw with an initiation time occurring before the "initiation end time." These flaws are "scheduled to initiate". Subsequently, the Monte Carlo realization enters the time looping structure.

The time looping structure is composed of an outer cycle-by-cycle loop with a nested within-cycle loop. The cycle-by-cycle loop may be terminated if all flaws that have been "scheduled to initiate" have been repaired. If this occurs, the program exits the time loop structure, stores relevant information, and cycles to the next Monte Carlo realization.

The within-cycle loop is entered if there is an active flaw whose initiation time is less than the time of the end of the current operating cycle. Immediately prior to entering the within-cycle loop, any peening application that is scheduled for the current cycle is invoked resulting in new stress profiles utilized to predict crack growth.

If no flaw initiations occur prior to the end of the current sub-step in the within-cycle loop, the sub-step is skipped. Otherwise, at the beginning of each sub-step, the stress intensity factor for each active flaw is calculated based on the geometry of the flaw and the stress profile at the beginning of the sub-step. During each sub-step, all active flaws are grown using the flaw propagation model (detailed in Section A.5) that determines the flaw propagation rate and increases the depth and length of the flaw at a constant rate for the duration of the sub-step.

Before completing a given sub-step, the program checks if any flaw has reached through-wall, and if so, the cycle number is stored for a statistical summary generated at the end of Monte Carlo run. The exception to this is if a flaw achieves through-wall crack growth before a user-defined past inspection time for which it is assumed that no flaws have leaked or been detected (i.e., credit is taken for the fact that the modeled DM weld has not leaked or had detected cracks up to a user defined time); in this case, the Monte Carlo realization is restarted with newly sampled values. For DM welds, when through-wall growth occurs (and its timing does not contradict the results of the assumed past inspection), the current realization is terminated and the program returns to the start of the main loop (contrary to RPVHPNs whose simulation continues to check for nozzle ejection).

At the end of each sub-step, if multiple flaws are active, the coalescence model (detailed in Section A.5.4) is used to consolidate circumferential flaws that are determined to be close enough to coalesce.

When all sub-steps during a given cycle have been completed, the program determines if an examination is to be performed at the end of the current cycle, and if the examination is to be ultrasonic (UT), eddy current (ET), or both. If so, the UT or ET inspection models (detailed in Section A.6) are called appropriately. If a flaw is detected, and its detection time does not contradict the results of the assumed past inspection, the flaw is repaired and the cycle number is stored for a statistical summary generated at the end of the Monte Carlo simulation; the examination continues to any other active flaws. In a similar fashion to a through-wall occurrence, if any flaw detection result contradicts the results of the assumed past inspection, the code exits the time looping structure without saving any results and restarts the current Monte Carlo realization from the beginning of the main loop. If a flaw is not detected, it remains active. After all scheduled inspections, the code returns to the cycle-by-cycle loop and continues to the next cycle or returns to the main loop if the cycle-by-cycle loop is complete.

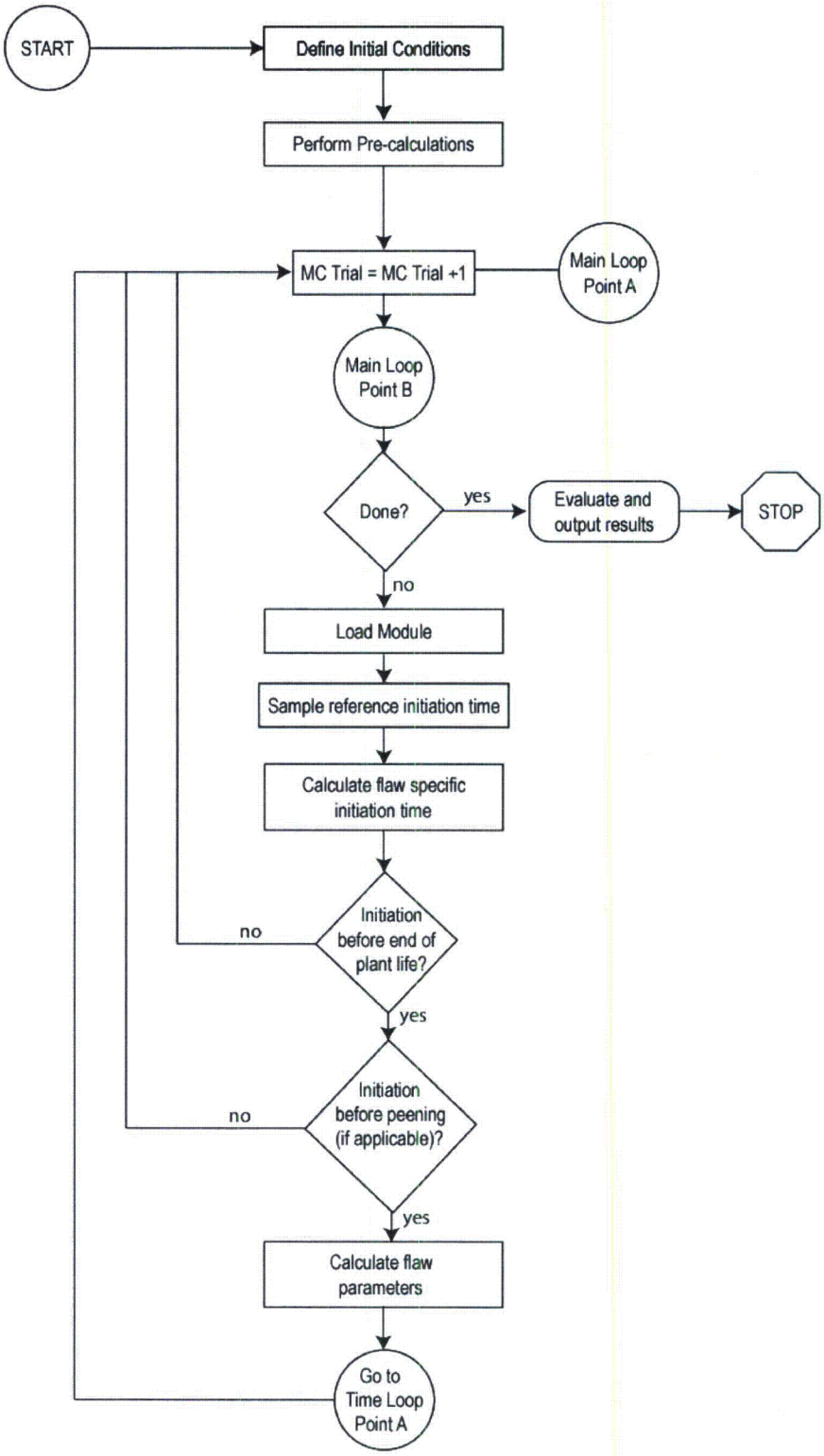

Figure A-1
DM Weld Probabilistic Model Flow Chart: Main Loop

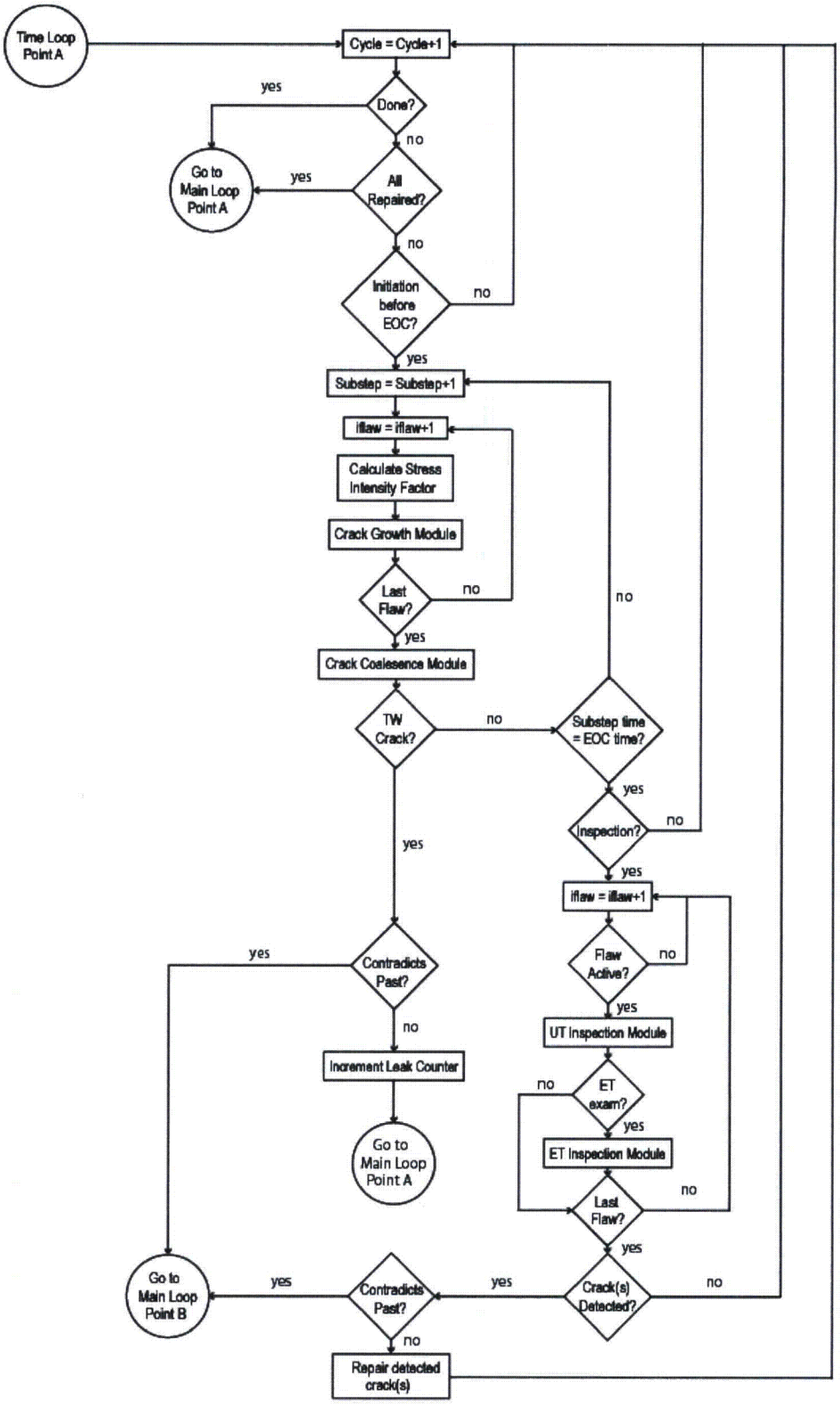

Figure A-2
DM Weld Probabilistic Model Flow Chart: Detail of Time Loop

A.3 Load and stress model

Load models are used to calculate the stress in the DM weld component during each Monte Carlo realization. The crack initiation and crack growth models utilize this information. Separate load models are used for hoop stresses (driving axial cracks) and axial stresses (driving circumferential cracks)[11].

The load models account for welding residual stresses, internal pressure, and piping loads (dead weight, thermal expansion, and thermal stratification, if applicable). In addition, a peening residual stress model is introduced for modeling crack growth during cycles after a peening application. The load models differentiate between residual stress and operational stress (which can all be combined to get total stress) as well as membrane stress and bending stress; the initiation and growth models use these differentiations at various steps.

The DM weld load models described in this report use many of the same general methodologies used by the xLPR Pilot Study program [2]. Significant differences between the models used in this study and those used in the xLPR Pilot Study include the following:

- Both axial and circumferential cracks are considered in this analysis. Because this study concentrates on the probability of through-wall crack growth and leakage rather than the probability of rupture, it was necessary to include axial flaws in the analysis.
- Peening residual stresses are modeled. The peening models are based on data and qualitative information provided by peening vendors (Hitachi-GE, Toshiba, MHI) as documented in MRP-267 Revision 1 [4]. These models are pertinent because the main goal of this report is to assess the impact of peening on component performance with respect to leak mitigation (and ejection mitigation for RPVHPNs).
- No seismic loads (which affect crack stability but not subcritical crack growth) are considered in the analysis reported here. For simplicity, the failure criterion in the current study was selected to be a through-wall crack. Therefore, demonstrated crack stability during seismic events is not relevant.
- Thermal stratification loads are not included in this study. The xLPR Pilot Study investigated PWSCC degradation for a pressurizer surge nozzle, and thus included thermal stratification loads.

In the same manner as for the xLPR Pilot Study, it is assumed that the residual stress profile does not vary around the circumference (i.e., all residual stresses are axisymmetric).

The methodologies for calculating stresses due to internal pressure and piping loads (operational loads), component welding, and peening are discussed in Sections A.3.1, A.3.2, A.3.3, respectively. Considerations for the effects of

[11] The subscripts "h" and "a" will be used to differentiate between hoop and axial stresses.

temperature and load cycling are discussed in Section A.3.4. The load model for initiation and growth is summarized fully in Section A.3.5.

A.3.1 Internal pressure and piping loads

Pipe stresses due to internal pressure, in the hoop and axial directions, are calculated using thin-walled cylindrical shell equations:

$$\sigma_{P,h} = \frac{PD_i}{2t} \qquad \text{[A-1]}$$

$$\sigma_{P,a} = \frac{PD_i^2}{(D_i + 2t)^2 - D_i^2} \qquad \text{[A-2]}$$

where P is the normal operating pressure, D_i is the pipe inner diameter, and t is the pipe thickness.

For both axial and circumferential cracks, a crack face pressure stress equal to the operating pressure, P, is superimposed after initiation.

Other piping loads include dead weight and pipe thermal expansion. These loads act to create a longitudinal force component, torsion, and two orthogonal bending moments. The contribution of these loads to hoop stress is neglected.

The axial membrane stresses due to deadweight and normal thermal expansion are calculated:

$$\sigma_{DW,a} = \frac{F_{DW}}{A} \qquad \text{[A-3]}$$

$$\sigma_{NTE,a} = \frac{F_{NTE}}{A} \qquad \text{[A-4]}$$

where F_{DW} and F_{NTE} are the axial loads due to dead weight and normal thermal expansion, respectively, and A is the cross-sectional area of the pipe.

The bending stress is calculated using the bending moment and torsion components of the dead weight and normal thermal expansion piping loads (i.e., M_x (torsion) and M_y and M_z (bending)). The load model determines an effective moment (M_{eff}) as a Von Mises combination of the bending and torsional loads:

$$M_{eff} = \sqrt{M_y^2 + M_z^2 + \left[\frac{\sqrt{3}}{2} M_x\right]^2} \qquad \text{[A-5]}$$

(For the calculation results presented in this appendix, the effective pipe moment acting on the weld cross section is an assumed input rather than calculated through this equation. Sensitivity cases are used to assess the effect of the magnitude of the effective moment, given its variability for actual plant components.)

Then, using the effective moment, the OD bending stress at any azimuthal angle (φ) is approximated as:

$$\sigma_B(\varphi) = \frac{M_{eff} R_o}{I} \cos(\varphi) \qquad \text{[A-6]}$$

$$I = \frac{\pi\left(R_o^4 - R_i^4\right)}{4} \qquad \text{[A-7]}$$

where R_o is the pipe outer diameter and I is the moment of inertia of the pipe cross-sectional area. Given this definition, φ=0° is the location of maximum tensile stress due to bending and φ=180° is the location of maximum compressive stress due to bending.

A.3.2 Welding residual stress before peening

The through-thickness residual stress profile is affected by local weld repairs and weld starts and stops. Thus, these processes can affect the susceptibility of the weld to initiation of PWSCC and the growth of PWSCC flaws through the weld, and as such must be modeled. In this analysis of DM welds, as in the xLPR Pilot Study, welding residual stress profiles are assumed to be axisymmetric and varying through-wall. The through-wall WRS profiles in the axial and hoop directions are detailed in the remainder of this section.

The axial load model uses a third-order polynomial function of through-wall fraction to approximate the axial WRS profile:

$$\sigma_{WRS,a}\left(\frac{x}{t}\right) = \sigma_{0,WRS,a} + \sigma_{1,WRS,a}\left(\frac{x}{t}\right) + \sigma_{2,WRS,a}\left(\frac{x}{t}\right)^2 + \sigma_{3,WRS,a}\left(\frac{x}{t}\right)^3 \qquad \text{[A-8]}$$

where x is through-wall depth from the inner diameter, $\sigma_{0,WRS,a}$ is the ID axial WRS stress, and $\sigma_{1,WRS,a}$, $\sigma_{2,WRS,a}$, and $\sigma_{3,WRS,a}$ are curve-fit parameters.

The model fits the three curve-fit parameters using three constraints (identical to those used in the xLPR Pilot Study) resulting in a system of three linear equations:

1. The OD axial WRS ($\sigma_{OD,WRS,a}$) is defined:

$$\sigma_{WRS,a}(1) = \sigma_{OD,WRS,a} \qquad \text{[A-9]}$$

2. A through-wall fraction at which axial WRS is zero (X_c) is defined:

$$\sigma_{WRS,a}(X_c) = 0 \qquad \text{[A-10]}$$

3. The axial WRS is constrained to equilibrate through the thickness of the wall considering the effect of curvature. Using the axisymmetric assumption, that is:

$$\int_0^t \sigma_{WRS,a}\left(\frac{x}{t}\right)(R_i + x)\,dx = 0 \qquad \text{[A-11]}$$

The circumferential load model uses a fourth-order polynomial function of through-wall percentage to approximate the hoop WRS profile:

$$\sigma_{WRS,h}\left(\frac{x}{t}\right) = \sigma_{0,WRS,h} + \sigma_{1,WRS,h}\left(\frac{x}{t}\right) + \sigma_{2,WRS,h}\left(\frac{x}{t}\right)^2 + \sigma_{3,WRS,h}\left(\frac{x}{t}\right)^3 + \sigma_{4,WRS,h}\left(\frac{x}{t}\right)^4 \qquad \text{[A-12]}$$

where $\sigma_{0,WRS,h}$ is the ID hoop WRS stress, and $\sigma_{1,WRS,h}$, $\sigma_{2,WRS,h}$, $\sigma_{3,WRS,h}$ and $\sigma_{4,WRS,h}$ are curve-fit parameters.

The model fits the four curve-fit parameters using four constraints resulting in a system of four linear equations:

1. The OD hoop WRS ($\sigma_{OD,WRS,h}$) is defined:

$$\sigma_{WRS,h}(1) = \sigma_{OD,WRS,h} \qquad \text{[A-13]}$$

2. The location of minimum hoop WRS (X_{min}) is defined:

$$\left[\frac{d}{dx}\sigma_{WRS,h}\left(\frac{x}{t}\right)\right]_{\frac{x}{t}=X_{\min}} = 0 \qquad \text{[A-14]}$$

3. The minimum hoop WRS ($\sigma_{min,WRS,h}$) is defined:

$$\sigma_{WRS,h}\left(X_{\min}\right) = \sigma_{min,WRS,h} \qquad \text{[A-15]}$$

4. The derivative of hoop WRS is assumed to be zero at the ID, effectively:

$$\sigma_{1,WRS,h} = 0 \qquad \text{[A-16]}$$

A.3.3 Residual stress after peening

As discussed in the body of this report, peening has the effect of adding a thin region of compressive stress in all three principal directions near the surface of its application. This compressive region both prevents crack initiation (assuming the surface stress below 20 ksi after superimposing operating stresses [5]) and slows the growth of cracks (especially shallow cracks). For modeling purposes, a single outage in the operating life of the plant can be selected for the application of peening. After the application, it is assumed that no new cracks initiate and the growth of existing cracks occurs in the presence of the post-peening residual stress (PPRS) profile described below.

As with WRS, the peening stress profile is assumed to be axisymmetric and varying through-wall. The through-wall PPRS, in both the hoop and axial directions, is modeled using a piecewise stress equation that captures the essential characteristics observed in the measured stress depth profiles reported in MRP-267 Revision 1 [4]. The vendor-supplied stress profile data are summarized in Table A-11 and Table A-12. The assumed PPRS profile shape is depicted in Figure A-3 and Figure A-4 and is described in the remainder of this section (using the symbols presented in the figures).

For modeling purposes, the post-peening profile is separated into four general regions: the compressive region (nearest to the peened surface), the first transition region, the second transition region, and the "minimally affected" region (farthest from the peened surface). These regions are presented out of spatial order below for pedagogical reasons:

Region 1: The Compressive Region

The compressive region is the thin region near the application surface where the hoop and axial residual stresses are made compressive. This region is characterized by a surface stress ($\sigma_{0,PPRS}$) and a penetration depth ($x_{1,PPRS}$). In this region, the PPRS profile varies linearly from the surface stress at the application

surface to neutral stress at the penetration depth, as is reflected in the following equation:

$$\sigma_{PPRS}(x) = \sigma_{0,PPRS} + \left(\frac{\sigma_{0,PPRS}}{x_{1,PPRS}}\right)x \qquad 0 \le x \le x_{1,PPRS} \qquad \text{[A-17]}$$

Note that the argument to the PPRS equations is absolute depth as opposed to the non-dimensional depth used by the WRS equations. This reflects the notion that the peening profile is insensitive to the thickness of the peening component (for thicknesses characteristic of components studied here).

The same surface stress and peening depth are applied to the axial and hoop directions. This reflects the assumption that the peening-induced pressure waves travel without dependence on their orientation to the peened component. Vendor-supplied data, including orthogonal stress profiles from the same peened component, support this assumption.

The assumption of a *linear* compressive region is supported by vendor-supplied peening profile data. Across 73 peening stress profiles (spanning different vendors, peening types, specimen types, etc.), 56 of the profiles fit with a linear curve yielded an R^2 goodness of fit metric greater than 0.75.

It is noted that the peening profile data from vendors uncovered a slight trend between the residual surface stress after peening and the residual surface stress prior to peening. This effect can be included in the model as a linear adjustment to the sampled PPRS surface stress value that is dependent on the residual surface stress before the peening application. This effect is not included for base case results.

Region 4: The "Minimally Affected" Region

The "minimally affected" region is the portion of the PPRS profile that is far enough (greater than the "minimally affected depth", $x_{3,PPRS}$) from the application surface that it does not experience a stress improvement. This region takes up the majority of the thickness of the component and is described by the following equations:

$$\sigma_{PPRS,a}(x) = \sigma_{WRS,a}\left(\frac{x}{t}\right) + A_a \qquad x_{3,PPRS} < x \le t$$

$$\sigma_{PPRS,h}(x) = \sigma_{WRS,h}\left(\frac{x}{t}\right) + A_h \qquad x_{3,PPRS} < x \le t \qquad \text{[A-18]}$$

The additive terms A_a and A_h are force balance terms included to ensure the effective residual force on the peened through-wall element does not change due

to peening (accounting for curvature for the axial stress case). Under the axisymmetric assumption, that is:

$$\int_0^t \sigma_{WRS,a}\left(\frac{x}{t}\right)(R_i + x)\,dx = \int_0^t \sigma_{PPRS,a}(x)(R_i + x)\,dx = 0$$
$$\int_0^t \sigma_{WRS,h}\left(\frac{x}{t}\right)dx = \int_0^t \sigma_{PPRS,h}(x)\,dx \qquad \text{[A-19]}$$

This modeling convention assumes that any residual tension removed near the application surface is redistributed elsewhere through-wall. The derivation of the force balance terms is withheld from this report for the purpose of conciseness, but is documented internally.

Regions 2 & 3: The Transition Regions

The two transition regions are used to connect the compressive region stresses with the "minimally affected" region stresses, preserving stress continuity through-wall. Because little information is available to describe this transition, a simple approach is taken.

The first transition region uses a linear equation to connect the neutral stress location at the penetration depth to the pre-peening residual stress at the "transition depth" ($x_{2,PPRS}$). The general equation for this is:

$$\sigma_{PPRS,d}(x) = \left(\frac{x - x_{1,PPRS}}{x_{2,PPRS} - x_{1,PPRS}}\right) \cdot \sigma_{WRS,d}\left(\frac{x_{2,PPRS}}{t}\right) \qquad x_{1,PPRS} < x \le x_{2,PPRS} \qquad \text{[A-20]}$$

where the subscript *d* indicates a placeholder for the subscript *a* (axial) or the subscript *h* (hoop).

The second transition region uses a linear equation to connect the pre-peening residual stress at the "transition depth" to the "minimally affected" region at the "minimally affected depth". The general equation for this is:

$$\sigma_{PPRS,d}(x) = \left(\sigma_{WRS,d}\left(\frac{x_{3,PPRS}}{t}\right) + A_d - \sigma_{WRS,d}\left(\frac{x_{2,PPRS}}{t}\right)\right)$$
$$\cdot\left(\frac{x - x_{2,PPRS}}{x_{3,PPRS} - x_{2,PPRS}}\right) + \sigma_{WRS,d}\left(\frac{x_{2,PPRS}}{t}\right) \qquad x_{2,PPRS} < x \le x_{3,PPRS} \qquad \text{[A-21]}$$

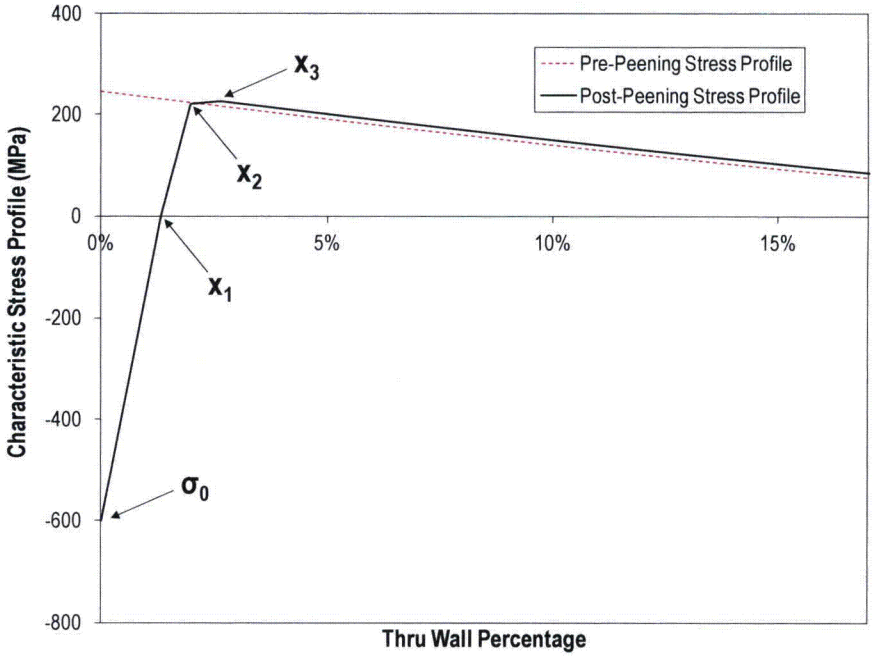

Figure A-3
Characteristic Stress Profile near Peened Surface

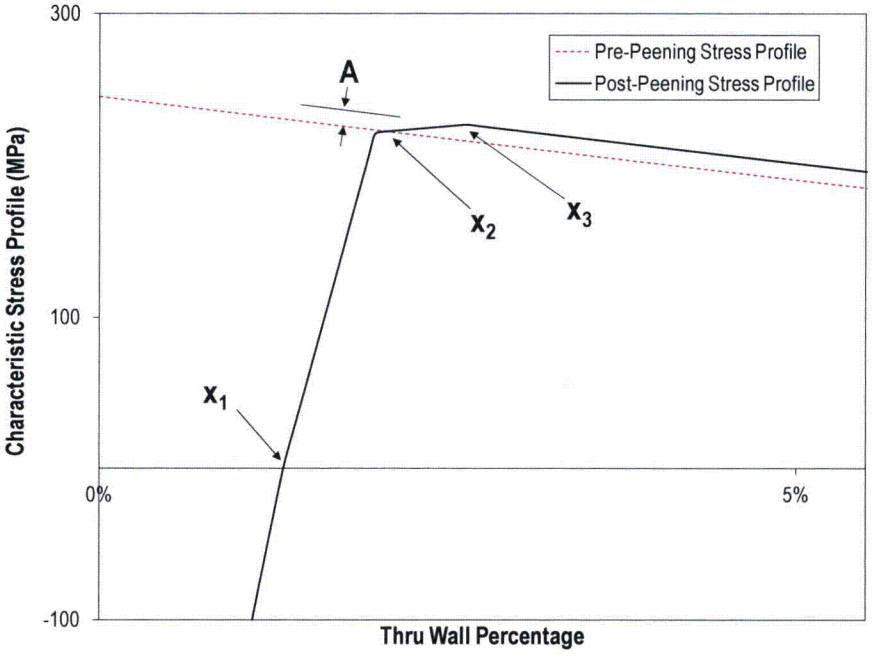

Figure A-4
Characteristic Stress Profile near Peened Surface: Detail of Transition Region

A.3.4 Effect of operating temperature and load cycling

Residual stress relaxation can occur in reactor components due to temperature and load cycling effects. This relaxation is characterized by a reduction of residual stress magnitudes as a function of operating time. This reduction may be especially important in this study because, if it is unaccounted for, the beneficial impact of peening residual compressive stresses may be overestimated for later cycles in a plant's operating life.

A simple and conservative approach is applied to model the relaxation of peening residual stresses. In this approach, a reduction factor, f_{relax}, is applied to the initial peening surface stress magnitude to account for relaxation that can occur over the life of the component:

$$\sigma_{0,PPRS} = f_{relax}\sigma_{0,PPRS}(t=0) \qquad \text{[A-22]}$$

The initial (unrelaxed) surface stress is based on vendor-supplied data for peened components not subjected to thermal or strain cycles. The relaxation factor is based on vendor-supplied data for peened samples subjected to strain cycling and/or elevated temperatures [4]. These analyses are detailed in Section A.8.5.

The use of this simple approach in lieu of a time-dependent stress relaxation model is not considered overly conservative. Experimental data predicts that a majority of the stress relaxation that will occur over the lifetime of a reactor head component, subjected to typical operational conditions, will occur very early (i.e., during the first cycle of operation).

It is noted that relaxation is not applied to welding residual stresses with this simple approach.

Other higher fidelity stress relaxation models were considered for implementation, but could not be justifiably fit to the wide scatter of available stress relaxation data. However, a best-fit time-dependent model is applied to peening and welding residual stresses in a sensitivity case presented later to better quantify the dependence of predicted results on the stress relaxation model.

A.3.5 Summary of load model

The models discussed in the previous sections can be combined to get total stress applicable to crack initiation or crack growth, before or after peening, and applicable to axial or circumferential cracks.

The DM weld *initiation* model considers only the surface (ID) stress and does not include crack face pressure. Prior to peening, this results in the following equations for axial and circumferential cracks:

$$\sigma_{ID,a}(\varphi) = \sigma_{P,a} + \sigma_{DW,a} + \sigma_{NTE,a} + \sigma_{0,WRS,a} + \frac{R_i}{R_o}\sigma_B(\varphi) \quad \text{[A-23]}$$

$$\sigma_{ID,h} = \sigma_{P,h} + \sigma_{0,WRS,h} \quad \text{[A-24]}$$

After peening, it is assumed that initiation cannot occur. That is, it is assumed that the compressive residual surface stress introduced by peening is sufficient to prevent the total surface stress during operation from reaching approximately 20 ksi(which is considered the threshold for formation of PWSCC [5]).

The growth model requires total stress as a function of through-wall depth. Prior to peening, the total stresses for axial and circumferential cracks are:

$$\sigma_{tot,a}(x,\varphi) = \sigma_{P,a} + \sigma_{DW,a} + \sigma_{NTE,a} + \frac{R_i + x}{R_o}\sigma_B(\varphi) + \sigma_{WRS,a}\left(\frac{x}{t}\right) + P \quad \text{[A-25]}$$

$$\sigma_{tot,h}(x) = \sigma_{P,h} + \sigma_{WRS,h}\left(\frac{x}{t}\right) + P \quad \text{[A-26]}$$

After peening, the total stresses for axial and circumferential cracks are:

$$\sigma_{tot,a}(x,\varphi) = \sigma_{P,a} + \sigma_{DW,a} + \sigma_{NTE,a} + \frac{R_i + x}{R_o}\sigma_B(\varphi) + \sigma_{PPRS,a}(x) + P \quad \text{[A-27]}$$

$$\sigma_{tot,h}(x) = \sigma_{P,h} + \sigma_{PPRS,h}(x) + P \quad \text{[A-28]}$$

Note that at most azimuthal locations on the pipe, the pressure and thermal loads that occur during operation result in a tensile contribution to stress. Superimposing these tensile operating stresses with the post-peening residual stress profile results in a reduced compressive stress and a reduced compressive layer depth at the peened surface stress. This is effectively captured in the equations above.

A.4 Crack initiation model

This study employs a statistical Weibull approach for predicting crack initiation and allows adjustments for operating temperature and surface stress, two factors commonly considered significant for crack initiation prediction. Furthermore, the

model allows for initiation of multiple flaws with axial or circumferential orientations.

A.4.1 Spatial Discretization of Crack Sites

In a similar fashion to the xLPR Pilot Study, to account for the possibility of multiple cracks, the DM weld component is divided into a 19 (N_{crack}) crack initiation locations. Because this study also analyzes axial cracks, each of the 19 crack *locations* is given both an axial and circumferential crack *site*. This results in 38 total crack sites at which initiation is modeled.

The program sets the crack locations simply by dividing the 360 degrees of the pipe ID into Ncrack equal arc lengths. By convention, the first crack location is centered at zero degrees, resulting in the following equation for the arc length centers (in radians):

$$\hat{\varphi}_i = \frac{2\pi}{N_{crack}}(i-1) \quad i = 1,..,N_{crack} \qquad \text{[A-29]}$$

where the subscript i will be used throughout the remainder of this appendix to denote the different crack locations.

After initiation, crack location is randomly sampled within its respective arc length.

A.4.2 Initiation Time for First Crack

A Weibull model has been selected for use in predicting the time of first initiation of PWSCC in DM welds. The use of this statistical model reflects systematic and statistical variations in material properties and environmental conditions from part to part. Furthermore, this statistical model captures the fact that the time between PWSCC initiation, for the population's first DM weld component and its last DM weld component, is quite long (several decades and even centuries). A number of distributions can be used to model failures, but the Weibull distribution is one of the most commonly used in reliability engineering since it can model a variety of data and life characteristics [5].

The two-parameter Weibull cumulative distribution function is given as follows:

$$F(t) = 1 - e^{-\left(\frac{t}{\theta}\right)^{\beta}} \qquad \text{[A-30]}$$

where F is the cumulative fraction of components with a PWSCC initiation and t is the corresponding operating time. The Weibull slope, or shape parameter, β, is related to the rate at which degradation spreads through a given component population such as steam generator tubing. The Weibull characteristic time

parameter, θ, provides a measure of the time scale for the degradation mode of interest. Specifically, the Weibull characteristic time is the time required to reach a cumulative failure fraction of 0.632 (i.e., the time required for 63.2% of the items in a given population to fail).

The Weibull slope, β, an arbitrary failure fraction, F_1, (e.g., 0.1%, 1%, 10%, etc.), and the time at which this arbitrary failure fraction is reached, t_1, are provided as inputs to the probabilistic model. The value of θ is then determined during runtime using Eq. [A-30]. The process by which β, F_1, and t_1 are fit to existing data for first crack initiation in DM welds is discussed in Section A.8.2.

Once β and θ are known for the current Monte Carlo realization, they can be used to sample a reference initiation time in EDY (t_{ref}). This sampled initiation can be adjusted to account for temperature, material condition, and feedwater chemistry. In this study, the initiation time is adjusted for temperature (to convert to EFPY) using the widely accepted Arrhenius relationship:

$$t_f = t_{ref} \times e^{\left(\frac{Q_i}{R}\right)\left(\frac{1}{T}-\frac{1}{T_{ref}}\right)} \qquad \text{[A-31]}$$

where T is the absolute operating temperature, Q_i is the apparent thermal activation energy for crack initiation, R is the universal gas constant, and T_{ref} is the Arrhenius model absolute reference temperature.

The result, t_f, is the time of the first PWSCC on the component for the current Monte Carlo realization. As a convention, this time is attributed to the crack located at the point of maximum tensile stress. If this point happens to be at a circumferential crack site, it will be at the location maximum tensile bending stress; if this point happens to be at an axial crack site, all of which experience the same tensile stress, the crack site is arbitrary (and the axial crack site located at 0° is selected). As described in the next section, the multiple flaw initiation model uses the first initiation time to predict the initiation times of the remaining crack sites.

A.4.3 Initiation Time for Multiple Cracks

A Weibull model has been selected for use in predicting times of initiation of multiple PWSCC cracks in a single DM weld component. The use of this statistical model reflects systematic and statistical variations in material properties and environmental conditions from location to location on a single component. An adjustment is made for surface stress at each location to capture the known dependence of PWSCC initiation susceptibility on surface stress.

The multiple crack initiation Weibull model uses a new Weibull slope, β_{mult}, or a new rate at which PWSCC degradation spreads to multiple sites on a component after the first crack initiation. This rate, when used to predict a time of initiation at each crack site independently, results in more rapid crack initiation than the time to first initiation model. This reflects the premise that there may be a

distinct, but random, event or condition that, after its onset, promotes more rapid PWSCC. This behavior has been observed in industry. The selection of a value for β_{mult} is discussed in Section A.8.2.

As in the previous section, a defined cumulative fraction at a defined time is necessary to complete the Weibull model. Since the time provided by Eq. [A-31] is indicative of the time of first PWSCC initiation across all $2N_{crack}$ crack sites, it is associated with the cumulative probability (F_{1st}) given in Eq. [A-32] below:

$$F_{1st} = \frac{1-0.3}{2N_{crack}+0.4} \qquad \text{[A-32]}$$

The shape parameter for the multiple flaw Weibull model, θ_{mult}, is calculated from β_{mult}, t_f, and F_{1st} above using Eq. [A-30]. Then, an initiation time for each remaining crack site, $t_{ref,i,d}$, is sampled from the resulting Weibull distribution. Sampled initiation times are truncated at t_f such that no cracks form prior to the crack at the site experiencing the largest tensile surface stress (i.e., if the initiation time sampled from the multiple flaw model is less than that of the first flaw, it is resampled).

Employing the surface stresses calculated by the load model (Eqs. [A-23] and [A-24]), each initiation time is adjusted for surface stress effects using an empirical stress-dependent factor ($S_{factor,i}$):

$$t_{f,i,d} = \frac{t_{ref,i,d}}{S_{factor,i,d}} \qquad \text{[A-33]}$$

$$S_{factor,i,a} = \left(\frac{\sigma_{ID,a}(\hat{\varphi}_i)}{\sigma_{ref}} \right)^n$$
$$S_{factor,i,h} = \left(\frac{\sigma_{ID,h}}{\sigma_{ref}} \right)^n \qquad \text{[A-34]}$$

where the stress exponent n and reference stress σ_{ref} are empirical parameters. Note that initiation times for sites with a compressive (negative) surface stress are not modeled with the above equations and instead the stress adjustment factor is considered to be zero; i.e., the initiation times are set to infinity; i.e., cracks are not allowed to initiate orthogonal to a compressive stress field.

By convention, the reference stress, σ_{ref}, is set equal to the stress at the site of maximum tensile stress. This constrains the stress adjustment factor in Eq. [A-34] to be less than or equal to one, across all crack sites, and effectively shifts initiation times for sites with lower stresses further into the future. This

normalizing convention has been selected over using a constant reference stress across all Monte Carlo realizations (as has been done in other studies) because it is assumed that the variation in the multiple flaw Weibull initiation models already includes the effects due to varying surface stresses throughout in-service DM welds. Thus, to apply Eq. [A-33] with a *constant* reference stress would be to "double-count" the variation due to component surface stress and, furthermore, would require an arbitrary selection of σ_{ref}.

A.4.4 Crack Initialization

Crack initialization refers here to assigning of initial conditions to each crack at its initiation time. These conditions include size, location, and capacity for growth. Orientation of an initiated crack, which has been part of initialization in other studies, is inherently addressed in the spatial discretization procedure discussed in Section A.4.1.

Initial crack depth is sampled from a distribution of positive, non-zero, crack through-wall percentages. This reflects both that the Weibull initiation models discussed above were fit to industry data recording first detection of crack indications and that crack detection is only possible for finite crack sizes. Initial crack lengths are attained by scaling the initial depth by a sampled aspect ratio.

Center crack location, φ_i, which is important in this study for modeling growth and coalescence of *circumferential* cracks only, is sampled uniformly on the arc length of each initiated crack, defined in Section A.4.1.

Finally, growth capacity for each crack is modeled using sampled growth variation terms, f_{weld} and $f_{ww,i}$, discussed in more detail in Section A.5.3. It is generally accepted by PWSCC experts that components and locations that are more susceptible to PWSCC initiation tend to have higher flaw propagation rates, even after normalizing for temperature and stress effects [21]. This tendency is modeled by correlating the weld-to-weld growth variation, f_{weld}, with the reference time of first PWSCC initiation, t_{ref}, and similarly by correlating the within-weld variation for each crack, $f_{ww,i}$, with the corresponding multiple flaw reference initiation time, $t_{ref,i}$.

A.5 Crack growth model

This study employs a model to allow the prediction of PWSCC growth rate as a function of crack geometry, component loading, and other conditions. Assuming that cracks maintain a semi-elliptical shape as they grow through-wall, the model predicts growth rates of the surface tips (in the length direction) and the deepest point (in the depth direction) of the crack.

The model predicts growth rates for partially through-wall cracks. As discussed in Section A.7, a through-wall growth (i.e., leakage) event is treated as the end condition in this study of DM welds, so growth prediction does not proceed to necessitate a through-wall crack growth model (contrary to the analysis of RPVHPNs).

Growth is simulated by integrating the crack growth rates over time. This integration is done numerically by discretizing each cycle into many sub-cycles and advancing growth linearly over each sub-cycle, using the crack geometry and stress profile at the beginning of each sub-cycle to predict growth rate (i.e., a forward Euler method).

The dependence of PWSCC on component loading (i.e., stresses near and orthogonal to the crack) requires the calculation of stress intensity factors at the crack points of interest. Sections A.5.1 and A.5.2 discuss the stress intensity factor calculation methods for a crack subject to a polynomial stress profile and a crack subject to a general stress profile, respectively. These solutions are based on the results of finite element parametric analyses for circumferential and axial cracks; these analyses are based on the superposition method of linear-elastic fracture mechanics.

The crack growth rate model, which factors in stress intensity factor, temperature, and various other effects, is discussed in Section A.5.3.

Finally, Sections A.5.4 and A.5.5 discuss special considerations made for predicting growth given geometry characteristics specific to a DM weld component and a stress profile characteristic of a peened component (i.e., with a compressive stress region near the surface), respectively.

A.5.1 Stress intensity factor calculation using influence coefficient method

Section 3 in Reference [8] describes the calculation of stress intensity factor, K, for a circumferentially or axially oriented surface crack on a pipe of arbitrary size using the influence coefficient method. The method described may be applied to a crack subjected to: a) a stress profile acting orthogonally to the crack face (i.e., axial stresses for circumferential cracks and hoop stresses for axial cracks) that is defined by a polynomial function in the direction of the crack depth and is uniform along the crack length, and/or b) stresses due to global bending loads, which are by definition not uniform over the crack length. (In this study, global bending loads are only considered for the growth of circumferential cracks.)

Before the application of peening, the axial and hoop residual stresses may be approximated by polynomial functions, as demonstrated in Equations [A-25] and [A-26], and so the influence coefficient method is used due to its simplicity and computational efficiency. After peening, the more general weight function method, which is described in the next section, must be employed.

The general form of the stress intensity factor calculation (for a surface crack with depth a on a pipe with thickness t) by way of the influence coefficient method is:

$$K = \left[\sigma_0 G_0 + \sigma_1 G_1 \left(\frac{a}{t}\right) + \sigma_2 G_2 \left(\frac{a}{t}\right)^2 + \sigma_3 G_3 \left(\frac{a}{t}\right)^3 + \sigma_4 G_4 \left(\frac{a}{t}\right)^4 + G_{gb}\sigma_{gb} \right] \sqrt{a\pi} \qquad \text{[A-35]}$$

where the G terms are the influence coefficients specific to the crack and component geometries and the point on the crack, σ_0 through σ_4 are the polynomial coefficients of the through-wall stress profile (in units of stress), and σ_{gb} is the nominal bending stress due to a bending moment acting in the direction indicated in Figure A-5 (i.e., the bending moment is assumed to be directed such that the crack center is at the azimuthal location of maximum tensile or compressive stress). While the bending direction indicated in Figure A-5 only applies to two distinct azimuthal locations on a pipe, stress intensity factors at all locations are calculated with Eq. [A-35] using bending stress approximated as a function of azimuthal angle per Eq. [A-6]. This is the same simplification made in the xLPR Pilot Study.

The influence coefficients are interpolated from tables built by way of linear-elastic finite element parametric analyses. Table 15 and 39 in Reference [9] provides such look-up tables for the surface tip and deepest points of cracks of interest to the study of PWSCC in DM weld components: semi-elliptical, axial or circumferential surface cracks on the inner diameter of a pipe. Higher order influence coefficients (e.g., G_2, G_3, and G_4) may be calculated with weight function coefficients as discussed in Section 6.3 in Reference [8].

The look-up tables for the crack types of interest require three non-dimensional terms: the ratio of the pipe inner radius to pipe thickness (R_i/t), the ratio of crack half-length to crack depth (c/a), and the ratio of crack depth to pipe thickness (a/t). Table A-1 describes the lower and upper bounds of the look-up tables provided in [9] and the protocol used for extrapolation of the look-up tables.

Table A-1
Interpolation and Extrapolation Criteria for Influence Coefficient Lookup

	R_i / t	c / a	a / t
Lower Bound	1	1	0
Lower Truncation Protocol	Error message is given. Extrapolation is not reliable below $R_i/t=1$.	Value of c/a=1 is used. Extrapolation is not reliable below c/a=1.	Error message is given. Negative depth indicates error.
Upper Bound	1000	16	0.8
Upper Truncation Protocol	User is instructed to use $R_i/t=1000$. Solution is converged to a flat plate	Value of c/a=16 is used. Extrapolation is not reliable above c/a=16.	Linear extrapolation of look-up table is executed.

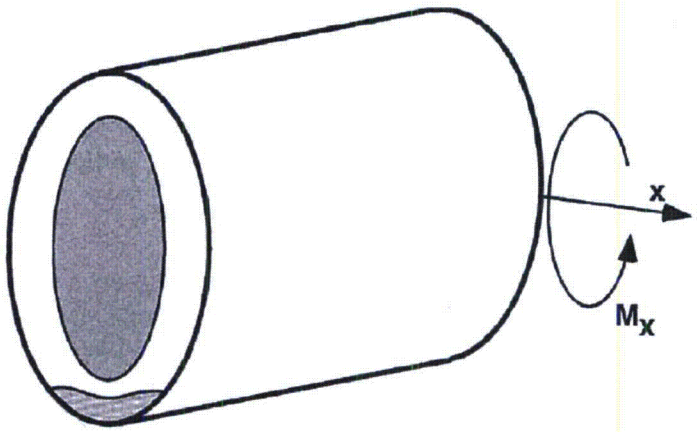

Figure A-5
Crack Location Relative to Bending Moment Assumed for Stress Intensity Factor Calculation [8]

A.5.2 Stress intensity factor calculation using the weight function method

Section 6 in Reference [8] describes the calculation of stress intensity factor, K, for a circumferentially or axially oriented surface crack on a pipe of arbitrary size using the weight function method, a generalization of the influence coefficient method discussed in the previous section. The weight function method may be applied to a crack subjected to a stress profile acting orthogonally to the crack face (i.e., axial stresses for circumferential cracks and hoop stresses for axial cracks) that is defined by an arbitrary function in the direction of the crack depth and is uniform along the crack length.

The general form of the stress intensity factor calculation by way of the weight function method is:

$$K = \int_0^a h(x,a)\sigma(x)dx \qquad \text{[A-36]}$$

where x is the distance from the surface, $h(x,a)$ is the weight function, and $\sigma(x)$ is the stress profile function. (The weight function is dependent on the crack and component geometries and the location on the crack although this is not demonstrated explicitly by its argument list for the sake of conciseness.)

For the purpose of predicting crack growth under the semi-elliptical crack shape assumption, the two points of interest on the crack are the deepest point (denoted by the subscript *90*) and the surface tip points (denoted by the subscript *0*). The general weight functions for these two points, respectively, are:

$$h_{90} = \frac{2}{\sqrt{2\pi(a-x)}}\left[1 + M_1\left(1-\frac{x}{a}\right)^{1/2} + M_2\left(1-\frac{x}{a}\right) + M_3\left(1-\frac{x}{a}\right)^{3/2} + M_4\left(1-\frac{x}{a}\right)^{2}\right] \quad \text{[A-37]}$$

$$h_0 = \frac{2}{\sqrt{\pi x}}\left[1 + N_1\left(\frac{x}{a}\right)^{1/2} + N_2\left(\frac{x}{a}\right) + N_3\left(\frac{x}{a}\right)^{3/2} + N_4\left(\frac{x}{a}\right)^{2}\right] \quad \text{[A-38]}$$

where the M and N terms are simple algebraic equations of the influence coefficients discussed in the previous section [10].

The weight function method is powerful because it allows the estimation of stress intensity factors for an arbitrary through-wall stress profile function. This capability is required in this study because the post-peening stress profile cannot accurately be represented by a polynomial.

There are several approaches to evaluating the integral in Eq. [A-36]. If the functional form of the stress profile, the integral may be solvable analytically. This approach has been implemented for the four-region piecewise polynomial stress profile defined for post-peening in this study (Eqs.[A-27] and [A-28]). This method is similar to approximating any arbitrary stress profile with piecewise linear equation, resulting in a closed-form solution [10], as is being considered for the next phase of xLPR.

To experiment with different stress profiles, without having to derive the analytical weight function indefinite integral for each, a numerical integration procedure is also available. An adaptive, open, degree-2, Newton-Cotes integration algorithm with a 1% convergence termination criteria is employed to estimate the weight function integral numerically (see Section 4.1 of Reference [3]). The use of an integral transformation discussed in Chapter 4.4 of Reference [3] accelerates convergence by concentrating the integrand evaluations in areas with the most rapid change (i.e., near the vertical asymptotes of the weight functions given in Eqs. [A-37] and [A-38]).

Due to the mathematical and programming complexities of the implemented weight function solution modules, verification studies were performed to compare stress intensity factor solutions against FEA Crack [11], for various crack geometries and stress profiles.

It is noted that the weight function method cannot be applied accurately for estimating stress intensity factors due to bending because the bending stress profile is by definition not uniform along the crack length. So, after the application of peening, the contribution of the global bending load to the stress intensity factor continues to be evaluated with the influence coefficient method

(as discussed in the previous section) and is superimposed with those stress intensities due to axisymmetric membrane stresses. Accordingly, for circumferential cracks, Eq. [A-36] becomes:

$$K = \int_0^a h(x,a)\sigma(x)dx + G_{gb}\sigma_{gb}\sqrt{a\pi} \qquad \text{[A-39]}$$

A.5.3 MRP-263 crack growth rate model for Alloy 182/82

The model selected in this study to estimate PWSCC crack growth in Alloy 182 weld metal is the model presented in MRP-263 [12].

The crack growth model provides a way to predict the extension of crack length and depth due to PWSCC. The model is relatively simple and incorporates the major factors affecting flaw growth rate: temperature and stress intensity factor. Temperature effects are incorporated through a widely accepted Arrhenius term and stress effects are incorporated through a standard power-law dependence, as presented below:

$$\frac{\delta}{\delta t}(d) = e^{-\frac{Q_g}{R}\left(\frac{1}{T}-\frac{1}{T_{ref}}\right)} \alpha f_{weld} f_{ww} \left(K_I - K_{Ith}\right)^b \qquad \text{[A-40]}$$

where

d	=	general crack dimension (e.g., depth or length)
Q_g	=	thermal activation energy for crack growth
R	=	universal gas constant
T	=	absolute temperature at location of crack
T_{ref}	=	absolute reference temperature used to normalize data
α	=	power-law coefficient
f_{weld}	=	common factor applied to all specimens fabricated from the same weld to account for weld wire/stick heat processing and for weld fabrication
f_{ww}	=	"within weld" factor that accounts for the variability in crack growth rate for different specimens fabricated from the same weld
K_I	=	crack-tip stress intensity factor at location of interest

K_{Ith} = crack-tip stress intensity factor threshold, below which the crack growth rate is zero

b = stress intensity factor exponent

This model is analogously applied to predict depth growth (substituting the K_{90} stress intensity factor term for the K_I term above) and length growth (substituting the K_0 stress intensity factor term for the K_I term above).

The estimation of crack growth versus time requires the solution of the above ordinary differential equation. This is achieved numerically by discretizing each plant operating cycle into many sub-cycles and advancing growth linearly over each sub-cycle, using the crack geometry and stress profile at the beginning of each sub-cycle to predict growth rate (i.e., a forward Euler method). The use of 12 sub-cycles per calendar year has been demonstrated to converge sufficiently to actual solution (e.g., a solution that uses twice as many sub-cycles) for a variety of initial conditions, temperatures, and stress profiles.

Various parameters in the above equation are empirical in nature and their derivation for crack growth in Alloy 182/82 is described in Section A.8.3. These include the absolute reference temperature T_{ref}, the growth activation energy Q_g, the power-law coefficient α, the crack-tip stress intensity factor threshold K_{Ith}, and the stress intensity factor exponent b.

Two additional factors, f_{weld} and f_{ww}, are included in the crack growth model to describe the aleatoric uncertainty in the crack growth rate model (i.e., uncertainty due to the unknowns that differ each time we run the same experiment). The within-weld variation, f_{ww}, is a value sampled for each flaw site from a distribution reflective of the growth rate variation observed in laboratory studies of cracks in a controlled weld. Similarly, the weld-to-weld growth rate variation, f_{weld}, is a value sampled for each weld from a distribution reflective of the growth rate variation observed in laboratory studies of cracks in identically controlled welds, after accounting for the within-weld variation. The derivation of these distributions is described in Section A.8.3.

As discussed in Section A.4.4, the sampled growth variation terms may be correlated with sampled initiation times to simulate the premise that components and locations that are more susceptible to PWSCC initiation tend to have higher flaw propagation rates.

A.5.4 Special considerations for crack growth on a DM butt weld geometry

This section discusses the special constraints and interactions applied to cracks growing on a DM weld component. These constraints and interactions are imposed by a set of modeling "rules" used to approximate known physical behaviors. While these physical behaviors are complex in nature, the simple set of rules is applied in the probabilistic model in order to capture the most essential growth characteristics.

As discussed in Section A.4.1, both axial and circumferential cracks are allowed to initiate on the inner diameter of the DM weld. Axial cracks are constrained such that they cannot grow beyond the defined width of the weld geometry. Circumferential cracks are constrained such that they cannot grow beyond the defined inner circumference of the weld geometry. In the rare case that an axial, or circumferential, crack grows the defined width, or circumference, of the weld before growing through-wall in the depth direction, it's length is truncated.

It is assumed that axial cracks do not interact with each other, or with circumferential cracks. This is a reasonable assumption given the large variability in weld residual stress and crack growth rates assumed in the probabilistic analyses.

Conservatively, all initiated circumferential cracks are assumed to initiate and grow on the same axial plane. Accordingly, it was necessary to develop a coalescence model, or a set of coalescence rules, to describe the crack interaction on this plane. These are described in the remainder of this section:

Coalescence is modeled at the completion of each sub-cycle growth prediction, if multiple circumferential cracks are active. Coalescence is considered to occur if, at the completion of a given sub-cycle, two adjacent cracks (call them cracks *A* and *B*) overlap or are close enough such that the dividing section of weld material collapses. While the phenomena of weld section collapse is highly complex, the collapse distance, $\Delta c_{threshold}$, is modeled here as a user-defined ratio, $1/F_{coalescence}$, of the maximum depth of cracks *A* and *B*:

$$\Delta c_{threshold} = \frac{\max\{a_A, a_B\}}{F_{coalescence}} \qquad \text{[A-41]}$$

where the subscripts *A* and *B* denote the two adjacent cracks. The same methodology is discussed in [13], where $F_{coalescence}$ is defined as 2.0.

If coalescence occurs, the following rules are used to consolidate the original cracks into a single resulting crack:

- The resulting crack is assumed to take on a semi-elliptical shape immediately following coalescence, with a depth equal to the maximum depth of cracks *A* and *B* and a length such that the original cracks *A* and *B* are fully circumscribed.
- The within-weld variation factor for the resulting cracks is calculated using a depth-weighted average of cracks *A* and *B*:

$$f_{ww,i} = \frac{a_A f_{ww,A} + a_B f_{ww,B}}{a_A + a_B} \qquad \text{[A-42]}$$

The within-weld variation is thought to be a function of varying material and chemical conditions. During coalescence, the resultant within-weld variation factor is considered to be dependent on the within-weld factors of the original cracks. This is because the resultant crack will grow in a combination of the material and chemical conditions of the original cracks. The depth-weighted average in Equation [A-42] gives preference toward the deeper crack, which on average is expected to have the higher of the two within-weld factors.

The coalescence of cracks is repeated until there are no active cracks close enough to one another (although it would be extremely rare for more than two cracks to coalescence during a given sub-cycle given the initiation rates discussed previously).

A.5.5 Special considerations for crack growth on a peened surface

This section discusses special considerations made for predicting growth in a component with a stress profile characteristic of a peened component, i.e., with a compressive stress region near the surface. The traditional stress intensity factor calculation methods discussed in Sections A.5.1 and A.5.2 assume a crack that is fully-open and semi-elliptical, while in fact, given a compressive stress region near the surface, these assumptions may be far from realistic. Two deviations from these assumptions, and how they are addressed from a modeling standpoint, are discussed in this section; they are crack closure and sub-surface, often resembling a "balloon" shape, crack growth. Both of these topics are highly complex and have been investigated in great detail in other empirical, numerical, and analytical studies. Discussion here is held relatively brief given the rarity of cracks remaining active (deeper than the compressive peening layer) after peening, and the marginal importance of these effects with respect to the growth of such cracks, as demonstrated in deterministic calculations provided in Section 5.2.

As has been emphasized throughout this report, peening produces a compressive layer near the surface that prevents crack initiation and slows crack growth. During operation after the application of peening, the depths of the compressive layer in the axial and hoop directions, $x_{comp,a}$ and $x_{comp,h}$, are given by the following equations:

$$x_{comp,a} = x_{1,PPRS}\left(1-\frac{\sigma_{oper,a}}{\sigma_{0,PPRS}}\right)$$
$$x_{comp,h} = x_{1,PPRS}\left(1-\frac{\sigma_{oper,h}}{\sigma_{0,PPRS}}\right) \qquad \text{[A-43]}$$

where $\sigma_{oper,a}$ and $\sigma_{oper,b}$ are terms that include all the operational stresses on the peened location of interest; if the operational stress is tensile, it has the effect of moving the compressive layer depth nearer to the surface.

Cracks with depths less than the compressive layer depth are considered to close entirely at the time of peening. Such cracks do not have any stresses acting to open their crack faces and thus are assumed to arrest. This is consistent with the results of laboratory experimentation of crack growth in a peened component [4].

Cracks with depths greater than the compressive layer may have partial closure, i.e., they are open at their deep crack tip, but may be closed near the surface due to the compressive layer (see Figure A-8). At locations where crack closure occurs, a contact stress is created that is considered to be equal and opposite to the local stresses. If the stress required to keep the crack closed is superimposed with the contact stresses (as in Figure A-8) it can be shown that the only stresses that contribute to crack stress intensity factor are those acting in regions where the crack remains open. As a corollary, if closure is not accounted for, stress intensity factors may be under-estimated, and in some cases they may be predicted to be negative or zero when in fact they are positive.

Reference [14] presents a methodology for accounting for crack closure under the assumption of elastic deformation of the crack face. This methodology has been implemented in this study. Because the methodology is iterative in nature and requires a substantial computational effort, it has been made optional. A sensitivity study is presented later to demonstrate the effect of crack closure on leakage probability.

A second special consideration for crack growth near a compressive surface stress is "balloon" crack growth: growth of PWSCC below the compressive layer near the surface, while growth is arresting in the compressive layer. For cracks with depths greater than the compressive layer depth, the effect of the peening stresses on the crack growth is inaccurately modeled solely by growing the crack at the surface (in length) and at the deepest point (in depth). Although the length of the crack at the peened surface may be held fixed, the sub-surface crack length (deeper than the compressive layer) can continue to grow.

To assess balloon-shaped growth, analyses were conducted using the finite element software FEA Crack to produce high fidelity predictions for crack growth, allowing for non-semi-elliptical growth (e.g., growth resembling a balloon), as seen in Figure A-6. (While the FEA Crack program simulates fatigue crack growth, advancing the crack front over load cycles instead of time, the resultant shape progression is reflective of the advancement of a PWSCC.) The crack shape results of these analyses were compared to two limiting cases; the first case did not allow crack length growth while the second allowed crack length growth uninhibited by peening. An example comparison of crack front shapes predicted the different methods is shown in Figure A-7. As expected, the balloon growth approximation bounds the length of the FEA predicted crack shape, given the same crack depth.

In a related study [15], it is demonstrated that crack growth below a PWSCC resistant weld inlay may be closely approximated by assuming a semi-elliptical shape below the inlay, driving growth with the deepest and surface points of sub-inlay portion of the crack (referred to as "idealized crack growth"). The idealized crack growth results in accurate time to through-wall crack growth relative to the actual crack growth predicted with FEA.

Considering these results, the "balloon" crack growth phenomenon is approximated conservatively by allowing crack length growth independent of peening (i.e., using only the pre-peening stresses). A sensitivity study is presented later to demonstrate the effect of fixing length growth after peening.

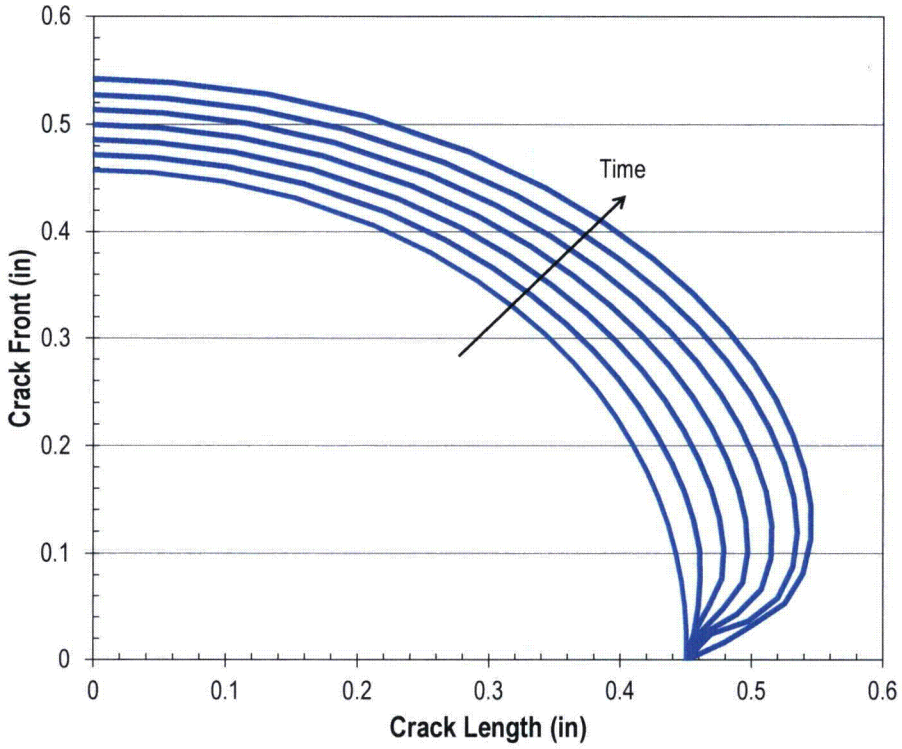

Figure A-6
Example of "Balloon" Crack Growth over Time Calculated with FEA Crack

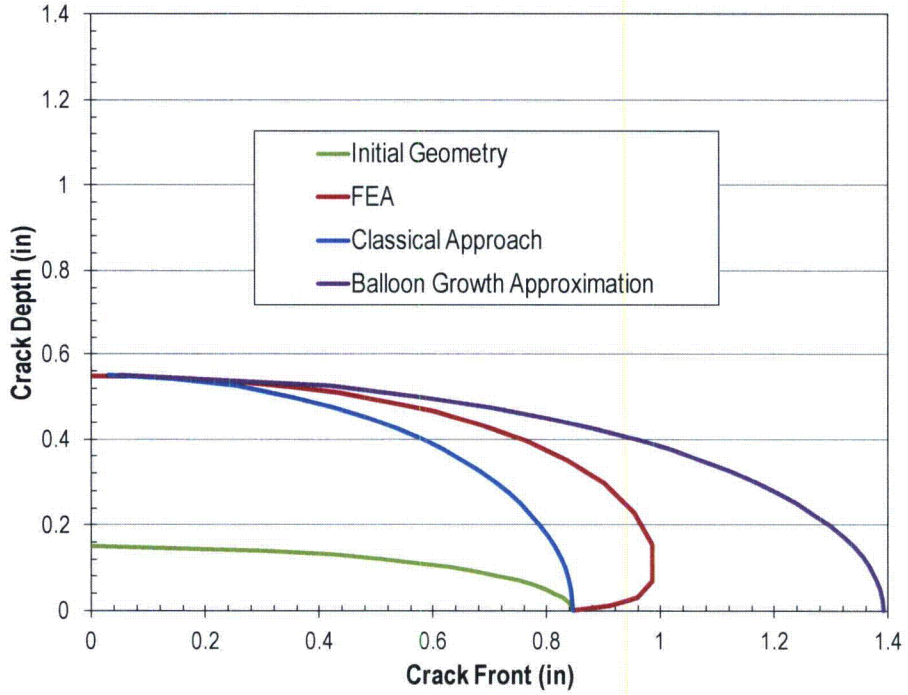

Figure A-7
Crack Front Shape for Different Growth Approaches

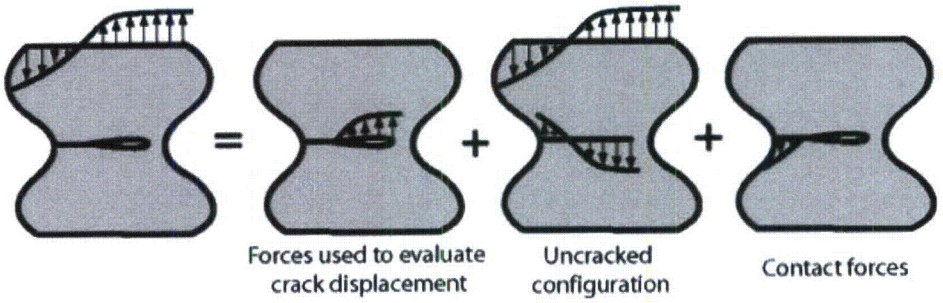

Figure A-8
Demonstration of Stresses Superposition for Partially Closed Crack

A.6 Examination models

This section describes the models applied to simulate ultrasonic and eddy current examinations of DM welds. Similar to the xLPR study, this study uses probability of detection (POD) curves to estimate the likelihood of a crack being detected, given its size. These models are essential for predicting leakage probabilities since cracks that lead to leaks are often those that go undetected during one or more scheduled examinations.

Section A.6.1 discusses how examinations are scheduled, before and after peening. Section A.6.2 describes the inspection models, i.e., how POD is

calculated, factoring for the geometry of the crack. Finally, Section A.6.3 describes the detection and repair modeling rules.

A.6.1 Examination Scheduling

UT examination scheduling for DM welds (prior to peening) is required per ASME Code Case N-770-1 [16]. Specifically, a Performance Demonstration Initiative (PDI) qualified volumetric inspection is required once every five years for unmitigated hot leg DM welds and once every seven years for hot leg cold leg DM welds. The time of the first modeled UT inspection is set by the user.

When peening is applied, different examination scheduling requirements and options are included in the model. First, during the peening application outage, immediately prior to peening, a UT inspection (and optionally an ET examination, or other ID surface examination) can be modeled to simulate a pre-peening inspection.

A follow-up UT examination is included before entering the relieved in-service inspection (ISI) schedule. In the comparative studies presented later, the follow-up inspection time is varied from 1 to 3 cycles after the peening application.

After the follow-up examination, a new ISI schedule is used. The central goal of this probabilistic modeling effort is to demonstrate that the ISI inspection interval after peening can be elongated compared to N-770-1 requirements without increasing the probability of leakage over the entire plant life. Accordingly, several different ISI intervals will be tested after peening and compared to predictions for unmitigated components.

A.6.2 Inspection Modeling

For modeling UT inspections of cracks in DM welds, the POD model from MRP-262 [17] will be used. This model is based on POD data for inspections of realistic DM weld mockups containing well-characterized, representative cracks.

The model from MRP-262 is comprised by a POD curve that is a function of the through-wall fraction of the crack, as given in the following equation:

$$POD\left(\frac{a}{t}\right)=\frac{e^{\beta_1+\beta_2\left(\frac{a}{t}\right)}}{1+e^{\beta_1+\beta_2\left(\frac{a}{t}\right)}} \qquad \text{[A-44]}$$

where β_1 and β_2 are fit parameters determined by regression analysis of inspection data from the mockups containing circumferential flaws. The specific values of these fit parameters are given in Section A.8.4. The resulting set of POD curves is demonstrated in Figure A-9.

The model defined in Eq. [A-44] is based on experiments which included circumferential cracks only. Experience gathered during UT detection

qualification suggests that POD may be lower in general for axial cracks. Accordingly, for axial cracks, an optional POD reduction factor, $f_{UT,axial}$, may be applied to the POD predicted by Equation [A-44].

The model defined in Eq. [A-44] is based on experiments including cracks ranging from 10% to 100% through-wall. The model is considered less reliable for small cracks (i.e., below 10% through-wall). To address this ambiguity, linear extrapolation is used between the origin (0% POD for an infinitesimal crack) and the POD given by Eq. [A-44] for 10% through-wall crack. (The model also includes the ability to set the POD to 0% for all cracks less than 10% through-wall; this option will be invoked in a sensitivity case to demonstrate the uncertainty in leakage probability predictions due to the unknown UT inspection efficacy for very small cracks.)

Similar to the UT inspection model, the ET inspection model uses a POD curve. However, there are several differences in the approaches because a) there are inherent differences in the examination techniques, and b) there is less data to support a ET detection model for cracks on DM welds. The differences are discussed below:

- For ET inspection, the POD is set to 0% for cracks below some half-length threshold, $c_{min,ET}$, regardless of the depth. This reflects the typical manner in which ET calls are made on the basis of more than one probe scan passed a position.
- For ET inspection, the POD curve is a function of crack depth, as opposed to through-wall fraction. This reflects the premise that ET inspections are insensitive to the thickness of the component (for thicknesses characteristic of DM welds).
- The ET inspection model is more general, providing a more transparent and expeditious way to define the uncertainty of the POD curve. This generality was desired given the scarcity of data for ET inspection of cracks on DM weld-type components. The general model is discussed for the remainder of this section.

The general POD model uses a lower bound and an upper bound POD curve, both of the following equation form:

$$POD_{ET}(a) = \frac{e^{\beta_{1,ET}+\beta_{2,ET}(\ln(a))}}{1+e^{\beta_{1,ET}+\beta_{2,ET}(\ln(a))}} \qquad \text{[A-45]}$$

where $\beta_{1,ET}$ and $\beta_{2,ET}$ are fit parameters determined by fitting an interpolating curve to two points, i.e., two pairings of depth size and POD. The pairings that were assumed in this study for the purpose of modeling the lower and upper bound ET inspection POD curves are discussed in Section A.8.4.3.

The lower and upper bound curves, $POD_{ET,U}$ and $POD_{ET,L}$, are assumed to represent the two sigma bounds for a stochastic family actual POD curves. To

get a single realization of the POD curve, a standard normal deviate, z_{ET}, is sampled once per Monte Carlo realization, and the following equation is used across all crack depths:

$$POD_{ET}(a) = \frac{POD_{ET,U}(a) + POD_{ET,L}(a)}{2} + z_{ET}\frac{POD_{ET,U}(a) - POD_{ET,L}(a)}{4} \quad \text{[A-46]}$$

Finally, for ET inspections, a maximum POD may be used, regardless of the crack size. This maximum POD is enforced to account for operator error or other potentials for random non-detection.

A.6.3 Detection and repair modeling

After a POD has been calculated, given the size of the crack of interest, detection may be simulated by sampling a random value between zero and one, referred to as the detection sample. If the detection sample is less than or equal to the POD, the crack is predicted to be detected; if not, the crack is predicted to be undetected for the current examination.

If the detection sample is sampled independently of previous samples, it reflects the premise that inspection success is uncorrelated, from examination to examination. Alternatively, the examination model allows for the correlation of successive detection samples for a given flaw. This is equivalent to assuming that each crack has some ambiguous features which may make it harder or easier to detect than the general population.

Credit can be taken for the condition that the unit(s) of interest have had no flaw detections before some user-defined past inspection time. If a flaw is predicted to be detected before this user-defined past inspection time, the Monte Carlo realization is rejected and repeated with newly sampled inputs. If a flaw is predicted to be detected after this past inspection time, that flaw is repaired (removed entirely from the flaw site), but the DM weld component stays in service and other flaws remain active.

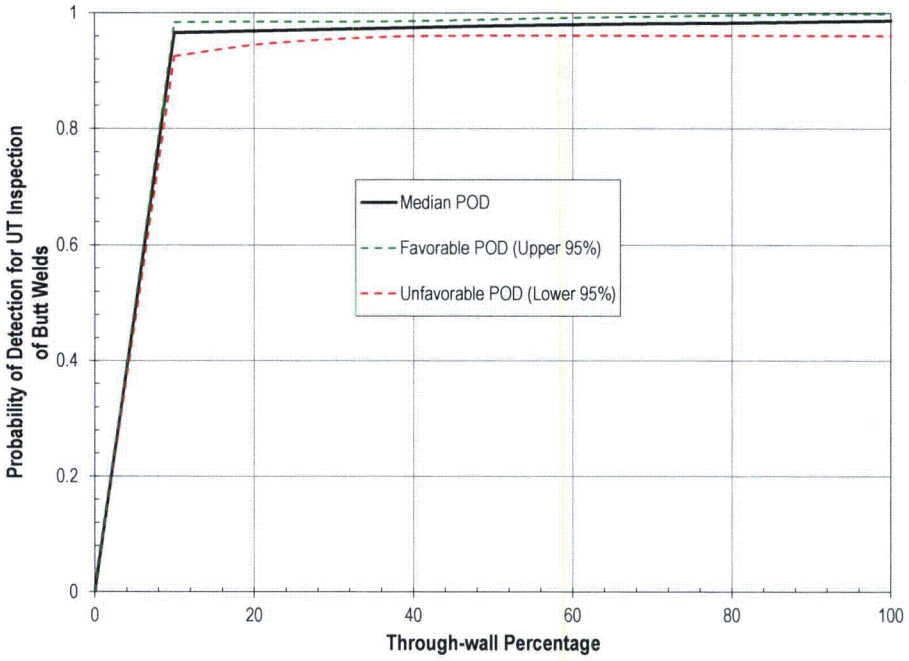

Figure A-9
UT POD for DMW ID Surfaces

A.7 Through-wall flaw (leakage) criterion

At the end of each Monte Carlo realization, the probabilistic model discussed in this report stores a limited number of metrics related to the extent of flaw growth and the repair status of the weld, including the timing of related events. Most importantly, during each realization, the code tracks if at least one flaw reaches through-wall crack growth (i.e., leakage) and, if so, the number of the cycle of the first through-wall crack growth.

Similar to detection, credit can be taken for the condition that the unit(s) of interest have had no leakages before some user-defined past inspection time. If a flaw is predicted to grow through-wall before this user-defined past inspection time, the Monte Carlo realization is rejected and repeated with newly sampled inputs, and the leak is not counted toward the metric discussed above.

Flaws modeled using the xLPR tool are able to reach through-wall crack growth either by propagating through the entire thickness of the component wall or by net section collapse of a critical surface flaw. Specifically, if the xLPR tool determines that the bending load on a given surface flaw exceeds the calculated net section collapse bending load, the surface flaw will transition to a through-wall flaw. For simplicity, the probabilistic model described in this report does not address the net section collapse failure mode and a given flaw may only reach through-wall crack growth if it propagates through the entire thickness of the wall before it is repaired.

One key metric of interest in the qualification of peening mitigation for DM welds is the probability of leakage cumulated over all cycles after the time of peening. This probability can be compared to the probability of leakage cumulated over the same period for an unmitigated component with no inspection relief. This comparison quantifies the relative difference in leakage risk for peened and unmitigated components.

A second metric of interest is the incremental probability of leakage during a given cycle, which is defined as the quotient of the number of realizations during which leakage occurred during a given cycle and the total number of trials. This is adjusted to a probability per year by dividing by the number calendar years per cycle.

For each Monte Carlo realization, a 60-yr plant life has been evaluated. This corresponds to the duration of an original license (40 years) plus an initial renewal (an additional 20 years). The cumulated probabilities of leakage are determined for this plant life value.

A.8 Probabilistic model inputs

The probabilistic modeling framework for DM welds takes both deterministic and distributed inputs. The values of the deterministic inputs are constant for every Monte Carlo realization. The values of the distributed inputs are determined by sampling probability distributions (e.g., normal distribution, log-normal distribution, triangular distribution, etc.) during each Monte Carlo realization. The probabilistic model accepts an array of eight inputs that is used to define the distribution of each distributed input. Each input array contains the following information:

- The value of the parameter to be used when conducting deterministic assessments;
- The distribution type to be sampled during probabilistic assessments (e.g., normal distribution);
- Parameter values defining the distributions (up to four, e.g., the mean and standard deviation of a normal distribution);
- Lower and upper truncation limits (selected using engineering judgment) used to impose bounds on the sampled values.

The inputs selected for use in the probabilistic model are discussed in Section A.8.1 through A.8.5. Note that unless otherwise specified, the six sigma bounds of the distribution of interest were selected for the upper and lower truncation limits when the normal or log-normal distribution was selected to describe the distribution of a given input parameter.

A.8.1 Component geometry, operating time, temperature, and loads

The choice of inputs for component geometry, operating time, temperature, and component loading are discussed in this section. These inputs are given for two

component cases for which results will be presented: a reactor vessel outlet nozzle (hot leg) in a Westinghouse plant and a reactor coolant pump nozzle (cold leg) in a B&W plant. Table A-2 tabulates the Westinghouse RVON component case inputs and Table A-3 tabulates the B&W RCP component case inputs.

A.8.1.1 Component Geometry

In similar fashion to the xLPR pilot study, the component specific parameters (i.e., wall thickness, outer diameter, and weld width) were taken as deterministic inputs. The values selected are for the outer diameter and the wall thickness are based on information provided in MRP-44 [18] and are given in Table A-2 and Table A-3.

A.8.1.2 Operating Time

Both DM weld components are simulated from plant startup until shutdown. Shutdown is considered to occur approximately 60 years after startup (i.e., a 40-yr original license and a 20-yr license renewal). Cumulative statistics are provided at the end of plant life.

Both DM weld components are simulated with 18-month operating cycles at a capacity factor of 0.92. These values are representative of US PWRs.

As discussed in the modeling sections, credit can be taken for the fact that the simulated component has not experienced leaks or repairs before some user-defined outage. Monte Carlo realizations that predict leaks or repairs before the user-defined outage are rejected and rerun with new samples. This option is not invoked for baseline results presented in this report. Accordingly, the cumulative probabilities that are presented are not conditioned on the assumption of no leakage or repair before some date, and can be thought of as applying to the general population of DM weld components with characteristics similar to those defined in Table A-2 or Table A-3.

As a sensitivity case, a user-defined outage (before which no leaks or repairs have occurred) will be set for the RPV outlet nozzle. The statistics presented in this study apply conditionally to Alloy 182 RPV outlet nozzles that have experienced no leaking or repairs to date, but otherwise have characteristics similar to those defined in Table A-2.

A.8.1.3 Temperature

Uncertainty in the component temperature is incorporated into the model by using a normal distribution. The temperature distributions used for the hot leg and cold leg nozzles are included in Table A-2 and Table A-3, respectively. The means of these distributions reflect maximums across active industry components. The uncertainty in the temperatures represent a number of factors including temperature streaming and measurement uncertainty. The standard deviations have been selected such that the 95% confidence band is ±5°C (±9°F) for the hot leg component and ±1°C (±1.8°F) for the cold leg component.

A.8.1.4 Loads

The input parameters specific to the DM weld loading are summarized in Table A-2 through Table A-4 and are further discussed below.

Like the xLPR Pilot study, relevant operational loads are taken as deterministic inputs. The values selected are considered to be representative of the loads in the actual components as described in MRP-307 [19]. Sensitivity studies are included to explore more extreme loading conditions.

Welding residual stresses are modeled stochastically. Uncertainty is incorporated into the calculation of welding residual stresses by setting distributions for parameters used to characterize and constrain the WRS profiles (Equations [A-9] through [A-16] present the constraint equations for the axial and circumferential WRS profiles). For the axial stress profile, the distributed inputs are the ID stress, the through-wall depth where the stress changes sign (from tensile to compressive) and ratio of the OD stress to ID stress. For the hoop stress profile, the distributed inputs are the ID stress, the location of the minimum stress, the ratio of the minimum stress to the ID stress, and the ratio of the OD stress to the ID stress.

The distributions for the parameters of the axial and hoop stress profiles are included in Table A-4. The distributions for the axial stress profile parameters are taken from the xLPR pilot study. The distributions for the hoop stress profile parameters were determined iteratively by using random sampling to generate a family of curves which adequately captured the uncertainty in the data as well as uncertainty due to missing data [19]. The truncation limits are used to prevent the occurrence of stress profiles deemed unrealistic by engineering judgment and experience.

Table A-2
Summary of Inputs Specific to RPV Outlet (hot leg) Nozzle

Symbol	Description	Source	Units	Distrib. Parameter	Value for Base Case
	Number of operating cycles	Selected to yield desired cumulative operating time	Nondim		53
	Nominal cycle length	Representative cycle length at Westinghouse plant	yr		1.5
CF	Operating capacity factor	Representative capacity factor for US PWR	Nondim		0.92
	EOC of first inspection	Selected based on median plant age and implementation time of MRP-139	Nondim		14
	EOC of assumed past inspection	Not used for base case study.	Nondim		N/A
	Inspection frequency	MRP-139	$(\#\ cycles)^{-1}$		3
t	Wall thickness of Westinghouse RVON-DMW	Representative component thickness	m		0.0699
D_o	Outer diameter of Westinghouse RVON-DMW	Representative component OD	m		0.9017
w	Width of Westinghouse RVON-DMW	Representative component width	m		0.0445
T	Operating temperature of Westinghouse RVON-DMW	Maximum Westinghouse hot leg operating temperature	°F	type	Normal
				mean	620.0
				stdev	4.6
				min	592.4
				max	647.6
P_{op}	Normal operating pressure	Representative normal operating pressure (P_{op} = 2,250 psi)	MPa		15.5
F_{DWx}	Average deadweight loads for Westinghouse RVON-DMW	Representative loads for Westinghouse plant	kN		0
M_{DWx}			kN-m		0
M_{DWy}			kN-m		0
M_{DWz}			kN-m		0
F_{NTEx}	Average normal thermal expansion loads for Westinghouse RVON-DMW	Representative loads for Westinghouse plant	kN		0
M_{NTEx}			kN-m		0
M_{NTEy}			kN-m		4519.4
M_{NTEz}			kN-m		0
	Component category for POD model	MRP-262 Table 8-1			B1

Table A-3
Summary of Inputs Specific to RCP (cold leg) Nozzle

Symbol	Description	Source	Units	Distrib. Parameter	Value for Base Case
	Number of operating cycles	Selected to yield desired cumulative operating time	Nondim		53
	Nominal cycle length	Representative cycle length at B&W plant	yr		1.5
CF	Operating capacity factor	Representative capacity factor for US PWR	Nondim		0.92
	EOC of first inspection	Selected based on median plant age and implementation time of MRP-139	Nondim		15
	EOC of assumed past inspection	Not used for base case study.	Nondim		N/A
	Inspection frequency	MRP-139	(# cycles)$^{-1}$		4
t	Wall thickness of B&W RCP Nozzle DMW	Representative component thickness	m		0.0737
D_o	Outer diameter of B&W RCP Nozzle DMW	Representative component OD	m		0.8585
w	Width of B&W RCP Nozzle DMW	Representative component width	m		0.0686
T	Operating temperature of B&W RCP Nozzle DMW	Maximum B&W cold leg temperature	°F	type mean stdev min max	Normal 554.0 0.9 548.5 559.5
P_{op}	Normal operating pressure	Representative normal operating pressure (P_{op} = 2,250 psi)	MPa		15.5
F_{DWx}	Average deadweight loads for B&W RCP Nozzle DMW	Representative loads for B&W plant	kN		0
M_{DWx}			kN-m		0
M_{DWy}			kN-m		0
M_{DWz}			kN-m		0
F_{NTEx}	Average normal thermal expansion loads for B&W RCP Nozzle DMW	Representative loads for B&W plant	kN		0
M_{NTEx}			kN-m		0
M_{NTEy}			kN-m		2259.7
M_{NTEz}			kN-m		0
	Component category for POD model	MRP-262 Table 8-1			B1

Table A-4
Summary of WRS-Specific Inputs for DM Weld Model

Symbol	Description	Source	Units	Distrib. Parameter	Value for Base Case
σ_{0WRSa}	Weld residual axial stress on ID surface	xLPR Input	MPa	type	Normal
				mean	300.3
				stdev	110.0
				min	150
				max	551
X_c	Fractional through-thickness at which weld residual axial stress profile crosses zero	xLPR Input	Nondim	type	Normal
				mean	0.25
				stdev	0.05
				min	0.125
				max	0.50
f_{WRSa}	Random scaling factor for weld residual axial stress on OD surface	xLPR Input	Nondim	type	Uniform
				min	0.50
				max	1.00
σ_{0WRSh}	Weld residual hoop stress on ID surface	xLPR Input	MPa	type	Normal
				mean	300.3
				stdev	110.0
				min	150
				max	551
X_{min}	Fractional through-thickness at which weld residual hoop stress is minimum	Iterative random sampling and engineering judgment.	Nondim	type	Normal
				mean	0.50
				stdev	0.075
				min	0.40
				max	0.75
f_{WRSh1}	Random scaling factor for minimum weld residual hoop stress	Iterative random sampling and engineering judgment.	Nondim	type	Normal
				mean	0.50
				stdev	0.10
				min	0.25
				max	0.75
f_{WRSh2}	Random scaling factor for weld residual hoop stress on OD surface	Iterative random sampling and engineering judgment.	Nondim	type	Normal
				mean	1.00
				stdev	0.075
				min	0.80
				max	1.20

A.8.2 Crack initiation model

The set of inputs for the DM weld PWSCC initiation model is described in Table A-5 at the end of this section. Various inputs are detailed in the following subsections.

A.8.2.1 Industry Inspection Data used to Develop Initiation Model

The following plant inspection data for piping to nozzle DM welds fabricated from Alloys 82 and 182 were used in the Weibull initiation model development:

- Pressurizer safety/relief nozzles, spray nozzles, surge nozzles;

- Reactor hot-leg piping surge nozzles, decay heat nozzles, drain nozzles, RV outlet nozzles, steam generator inlet nozzles, and shutdown cooling nozzles;
- Reactor cold-leg piping letdown drain nozzles, core flood nozzles, high-pressure injection nozzles, RCP suction and discharge nozzles, inlet nozzles, and safety injection nozzles.

Table A-6 shows the list of DM welds in which indications of cracking were detected that was used for this analysis. The data were compiled from industry documents (primarily documents from the NRC website such as LERs) using Table E-1 of MRP-216 [20] as a guide. Please note the following regarding Table A-6:

- All of the data are for U.S. plants
- No exhaustive effort was made to include all inspections of PWR piping DM welds that resulted in no indications being reported. This conservatively results in a higher probability of crack initiation than would have been the case if additional inspections were considered.
- The 17 nozzles given in Table A-6 were evaluated in detail and are considered either to be representative of service-induced cracking or it was not possible to rule out the presence of service-induced cracking (as opposed to fabrication-related defects, etc.). The remaining nozzles without indications are treated as suspended items [5] in the Weibull analysis.

Some of the welds inspected were without indications of cracking and are treated as suspensions. Specifically, a given weld that was found not to have any indications of cracking during its most recent inspection is modeled to have been removed from the statistical population at the time of the most recent inspection. The inspection data given in Table A-6 represent a summary of the detected flaws, which are part of what is known as a censored sample. For a Weibull distribution with a censored sample (i.e., failure data plus suspension data), it is necessary to account for the suspension times within the data set. Using the censored data set, it is possible to include the effect of the effective operating times of the uncracked components.

A.8.2.2 Weibull Fitting Procedure for Time of First Initiation

After adjusting the operating time data for the effect of operating temperature using the Arrhenius adjustment, the values of the Weibull parameters, β and θ, were determined using a maximum likelihood estimator (MLE) statistical procedure [5] fit to the PWR dissimilar metal weld experience. The MLE procedure is preferred over a least-squares fitting procedure in the case that limited cracking experience is available.

For the particular case of a Weibull distribution with a censored sample (i.e., failure data plus suspension data), the maximum likelihood estimates of the Weibull parameters β and θ may be determined by simultaneously solving the following equations:

$$\frac{\sum_{i=1}^{n} x_i^{\beta^*} \ln x_i}{\sum_{i=1}^{n} x_i^{\beta^*}} - \frac{1}{r}\sum_{i=1}^{r} \ln x_i - \frac{1}{\beta^*} = 0 \qquad \text{[A-47]}$$

$$\theta^* = \left(\frac{\sum_{i=1}^{n} x_i^{\beta^*}}{r} \right)^{\frac{1}{\beta^*}} \qquad \text{[A-48]}$$

where

β^* = maximum likelihood estimate of β

θ^* = maximum likelihood estimate of θ

x_i = operating time of component i

n = number of components in the population

r = number of failures

Components censored at times t_i are assigned values $x_{r+i}=t_i$. Thus, the second term in Equation [A-47] sums the logarithms of the failure times only. The values of β^* and θ^* may be found using an iterative procedure.

A least squares fitting procedure may also be used to determine the values of the Weibull slope and characteristic life parameters. This procedure consists of fitting the available data to the linearized representation of the Weibull distribution (see Equation [A-49]) using a least squares analysis.

$$\ln\left(-\ln(1-F)\right) = \beta\ln(t) - \beta\ln(\theta)$$
$$y = mx + c \qquad \text{[A-49]}$$

Specifically, a plot of F versus t on a double log-log plot yields a line with slope β. The value of θ may then be determined using the values of β and the vertical intercept (referred to here as c) obtained from the fit.

A.8.2.3 Analysis Results for Time of First Initiation

Figure A-10 shows an example MLE Weibull distribution fit to the industry experience with DM welds fabricated form Alloys 82 and 182 given in Table A-6. The failure and suspension times were adjusted to a common reference

temperature of 315°C using a thermal activation energy of 184 kJ/mole (the mean value given in Section A.8.2.10).

Table A-7 summarizes the MLE fit parameters of the Weibull analysis. Also included in Table A-7 are the standard errors in the Weibull fit parameter, β, and the vertical intercept of the linearized model determined from the linear least squares fit (which is used to determine the value of θ).

It is noted that for simplicity, the standard errors of the linear least squares parameters are presented instead of the MLE parameter values. It is also noted that the standard error in the vertical intercept of the linearized Weibull fit (referred to here as σ_c) is presented because it is used during runtime to account for the uncertainty in the value of the anchor point time, t_1, as discussed later.

A.8.2.4 Uncertainty in First Initiation Time Weibull Slope

The uncertainty in the Weibull slope, β, is modeled with a normal distribution having the mean and standard deviation given in Table A-7. The mean was selected as the value calculated using the MLE fitting procedure and for simplicity, the standard deviation was selected as the standard parameter error determined using the least squares fitting procedure. Based on the similarity of the Weibull slopes calculated using the two methods, this simplification is considered reasonable.

A.8.2.5 Uncertainty in Anchor Point Time (t_1)

Based on data presented in Figure A-10, a value of 0.01 was selected as the value of the arbitrary failure fraction, F_1. Figure A-10 shows that this failure fraction provides a reasonable representation of the earlier failures observed in the field, which will provide a more realistic set of Weibull curves defined by random sampling during the Monte Carlo analysis. That is, appropriately selecting the value of F_1 (which in combination with the Weibull slope and characteristic life determines the mean value of the anchor point time, t_1) will reduce the probability that the initiation model will greatly under-predict or over-predict (relative to observed plant experience) the initiation time of the first flaw during a given Monte Carlo realization.

The value of t_1 is determined by solving Equation [A-30] for time at a failure fraction of F_1 and the mean vales of the Weibull parameters, β and θ, given in Table A-7.

Uncertainty in the anchor point time is incorporated for each Monte Carlo realization using the following procedure:

- Determine the characteristic time, θ, using the value of F_1 and the deterministic values of β and t_1.
- Determine the mean intercept parameter, c, using the deterministic value of β and the value of θ determined in the previous step.

- Sample the value of c from a normal distribution using the mean intercept parameter determined in the previous step and the standard error (σ_c) given in Table A-7.
- Determine the anchor point time for the current trial using the sampled value from the previous step and the deterministic value of β.

A.8.2.6 Uncertainty in the Multiple Flaw Weibull Model

As discussed in the modeling section, a second Weibull model is used to predict the initiation of multiple flaws on a single component. The key inputs to this model are the Weibull slope and the empirical stress exponent.

Based on analysis of laboratory data, an empirical stress exponent, n, of about 4 is often assumed to describe the stress dependence of the initiation of PWSCC in Alloy 600 [7]. For this study, this exponent value is inherited for modeling PWSCC initiation in Alloy 182/82. A normal distribution with a mean of 4.0 standard deviation of 1.0 is employed to incorporate the uncertainties due to material and manufacturing disparities. A lower truncation bound of 0.0 is used to prevent the unphysical trend of earlier initiation for lower tensile surface stresses.

The Weibull slope of the multiple flaw model, β_{flaw}, quantifies the rate at which flaws occur after the initiation of the first flaw. An analytical data fitting procedure, as done for the first initiation time model, was not considered appropriate to fit β_{flaw} given the modeling complexities involved in sampling multiple flaw initiation times. Instead, a mean value of 2.0 was selected for β_{flaw}. This value has a precedent in probabilistic modeling of SCC in steam generators [7]. A normal distribution with a mean of 2.0 and a standard deviation of 0.5 is employed to incorporate uncertainties due to material and manufacturing disparities. A lower truncation bound of 1.0 was selected t0 prevent a multiple flaw Weibull model in which the PWSCC initiation rate decreases over all time.

A numerical experiment was run with a value of 2.0 for β_{flaw} in order to demonstrate the resulting number of cracks per component, given the parameter and stress distributions discussed throughout this Section A.8. Figure A-11 depicts the resulting distribution of number of flaws in components with at least a single flaw, at 20 EFPY, given an operating temperature of 600°F. The average number of flaws at 20 EFPY, given that at least a single flaw exists, is 4.8.

Industry experience shows that there have been up to three detected cracking indications on a single hot leg DM component, with the average close to 1.25 indications per component with at least a single flaw. These values are regarded as low given the existence of small cracks that have not been identified. Accordingly, the results given in the numerical study are not considered excessively conservative.

A.8.2.7 Uncertainty in Flaw Orientation

Flaw orientation is not directly controlled with a probability distribution. Rather, the stress adjustment together with the surface stress distributions dictates the ratio of flaw orientations.

A.8.2.8 Uncertainty in Initial Flaw Depth

The initial through-wall fraction for each flaw location is sampled at the time of flaw initiation. Since the PWSCC initiation model is based on in-service inspection results, the distribution of initial flaw through-wall fraction was defined using the expected sensitivity of the UT inspection technique. Specifically, the inspection data which provide the basis for the POD curves provided in A.8.4.2 predict that the POD for a 10% through-wall flaw is on the order of about 90%. When the POD curves are extrapolated backward to the origin, they predict a probability of approximately 50% of detecting a 5% through-wall flaw.

A log-normal distribution with a median of 5% of through-wall was selected to model the uncertainty in the initial flaw depth. The log-normal distribution conservatively provides greater weight for the upper end of the initial depth distribution (i.e., a long tail). The 95% confidence bound of the distribution was set to an initial depth of 10% through-wall as it is considered unlikely that a newly initiated flaw would be much deeper than 10% through-wall. The log-normal standard deviation was determined using the median and 95% confidence bound values specified above.

A lower truncation limit was defined to prevent the initiation of very small flaws for which the stress intensity factor (based on the input distributions of the surface welding residual stress) would be significantly less than the range of stress intensity factors (about 15-20 MPa $m^{1/2}$ or 14 to 18 ksi $in^{1/2}$) evaluated in the laboratory studies used to define the flaw propagation models given in MRP-115 [21] and MRP-263 [12].

The sensitivity results section presents a study in which the flaw through-wall fraction distribution is scaled down such that cracks initiate approximately 10 times smaller. This is included to assess the potential effect on leakage probability of smaller cracks not being identified during inspections prior to entering relieved inspection schedule after peening.

A.8.2.9 Uncertainty in Flaw Aspect Ratio

The distributions of the initial aspect ratios of axial and circumferential flaws were determined from the population of in-service inspection data discussed in A.8.2.1. The aspect ratio of a given flaw was calculated by dividing its total length by its depth. These data were used to determine approximate distributions of the axial and circumferential initial aspect ratios.

A log-normal distribution was selected to model the uncertainty in the initial aspect ratio of both circumferential and axial flaws because they provide

reasonable fits to the aspect ratio data given in Table A-6. The parameter values defining these distributions are given in Table A-5. It is noted that two axial flaws were not used to determine the distribution of initial aspect ratio:

- An axial flaw had propagated through-wall prior to detection. It was therefore excluded from the determination of the initial axial flaw aspect ratio distribution.
- The excavation depth of the axial flaw in the Plant AX surge nozzle was reported instead of the flaw depth. Rather than attempting to estimate the depth of the flaw based on the excavation depth, this flaw was excluded from the distribution of the initial flaw aspect ratio for axial flaws.

A.8.2.10 Uncertainty in Temperature Effect

Uncertainty in the apparent activation energy for PWSCC crack initiation is treated by defining a distributed input. As shown in Table A-5, a normal distribution is assumed to describe the uncertainty in the activation energy.

An activation energy of 209.4 kJ/mole is a standard value applied for the initiation of PWSCC in Alloy 600 components [22]. This value is based on evaluations of PWSCC in Alloy 600 steam generator tubing [23]. A lower, experimentally determined value of 184.2 kJ/mole was determined for Alloy 600 CRDM nozzle (i.e., thick-wall) material [24]. Due to similarities in the compositions of Alloys 82 and 182 and Alloy 600 wrought material, it is assumed that the range from 125.6 kJ/mole to 201.0 kJ/mole were reported in a review of activation energies determined from analyses of laboratory and field data [23]. Based on this discussion, 184.2 kJ/mole was selected as the mean of the distribution and the standard deviation was selected such that the 95% confidence bound of the distribution would be 209.4 kJ/mole.

Table A-5
Summary of Inputs for DM Weld Initiation Model

Symbol	Description	Source	Units	Distrib. Parameter	Value for Base Case
Q_i	Thermal activation energy for PWSCC flaw initiation	Q distribution based on laboratory data and judgment from experience with Weibull analysis	kJ/mole	type	Normal
				mean	184.23
				stdev	12.82
				min	107.32
				max	261.13
β	Weibull slope for PWSCC flaw initiation	Flaw initiation data assessed in this report	Nondim	type	Normal
				mean	1.055
				stdev	0.111
				min	0.389
				max	1.721
F_1	Arbitrary failure fraction selected to define Weibull PWSCC initiation function	Selected to reflect failure fractions observed for plant data	Nondim		0.01
t_1	Time at which failure fraction F_1 is reached	Flaw initiation data assessed in this report	EDY	type	Normal
				mean	19.8
				stdev	see σ_c
				min	1.93
				max	202.7
σ_c	Standard error in intercept of linearized Weibull fit	Linearized Weibull fit to flaw initiation data assessed in this report	ln(EDY)		0.409
T	Component operating temperature	See component-specific tables in this report	°F		
$T_{ref,i}$	Reference temperature to normalize PWSCC flaw initiation data	Temperature used to adjust flaw initiation data assessed in this report	°F		600.0

Table A-5
Summary of Inputs for DM Weld Initiation Model (continued)

Symbol	Description	Source	Units	Distrib. Parameter	Value for Base Case
N_{crack}	Number of circumferential locations for crack initiation	xLPR Pilot Study	Nondim		19
β_{flaw}	Weibull slope for PWSCC multple flaw initiation	Based on representative value for formation of PWSCC at multiple locations in industry SGs	Nondim	type	Normal
				mean	2.0
				stdev	0.5
				min	1.0
				max	5.0
n	Flaw initiation stress exponent	Experimental data from PWSCC laboratory testing in high-temperature water	Nondim	type	Normal
				mean	4.0
				stdev	1.0
				min	0.0
				max	10.0
σ	Maximum total stress at material surface	Load model	MPa		calculated by load models
σ_{ref}	Reference maximum total surface stress	Maximum surface stress across all crack sites	MPa		calculated by load models
a_0/t	Initial depth assigned to newly initiated flaw over wall thickness	Initial depth distribution based on expected sensitivity of inspection technique and flaw initiation data	Nondim	type	Log-Normal
				linear μ	0.053
				log-norm μ	-3.00
				log-norm σ	0.35
				min	0.0250
				max	0.42
AR_{circ}	Initial aspect ratio assigned to newly initiated circumferential flaw	Flaw initiation data assessed in this report	Nondim	type	Log-Normal
				linear μ	11.28
				log-norm μ	2.159
				log-norm σ	0.7271
				min	0.1104
				max	679.7
AR_{ax}	Initial aspect ratio assigned to newly initiated axial flaw	Flaw initiation data assessed in this report	Nondim	type	Log-Normal
				linear μ	3.44
				log-norm μ	0.554
				log-norm σ	1.167
				min	0.0016
				max	1912.2

Table A-6
Summary of Flaw Detection Experience in PWR Piping Nozzle Dissimilar Metal Welds

Plant	Component Type	Inspection Operating Time (EFPY)	Operating Temperature (°F)	Orientation	Component Wall Thickness (t, in.)	Axial Indication Depth (a, in.)	Axial Indication Total Length (2c, in.)	Axial Indication a/t	Axial Indication Aspect Ratio (2c/a)	Circumferential Indication Depth (a, in.)	Circumferential Indication Total Length (2c, in.)	Circumferential Indication a/t	Circumferential Indication Aspect Ratio (2c/a)
Plant D	CL Drain	21.7	545.0	Axial	0.6	--	--	--	--	--	--	--	--
Plant BL	CL Drain	17.6	555.0	Axial	0.6	0.06	≥ 0.25	7.0%	≥ 4.46	--	--	--	--
Plant D	HL Drain	21.7	597.0	Axial	0.6	0.39	--	70.0%	--	--	--	--	--
Plant AX	HL Surge	19.2	601.0	Axial	1.1	0.48	--	45.2%	--	--	--	--	--
Plant AB	HL Drain	23.1	597.0	Circ	0.5	--	--	--	--	0.10	0.45	19.0%	4.50
Plant AB	HL Surge	23.1	597.0	Circ	1.6	--	--	--	--	0.40	2.40	25.0%	6.00
Plant BK	Decay Heat	21.6	601.0	Circ	1.3	--	--	--	--	0.90	10.00	68.6%	11.11
Plant BL	Decay Heat	19.2	605.0	Axial	1.3	1.25	1.75	100.0%	1.40	--	--	--	--
Plant X	RPV Outlet	16.5	621.0	--	--	--	--	--	--	--	--	--	--
Plant Y	RPV Outlet	15.6	621.0	--	--	--	--	--	--	--	--	--	--
Plant N	Spray	13.9	653.0	Axial	0.89	0.21	0.25	24.0%	1.17	--	--	--	--
Plant V	Safety Relief	17.9	653.0	Circ	1.3	--	--	--	--	0.34	11.50	25.8%	33.82
Plant V	Safety Relief	17.9	653.0	Circ	1.3	--	--	--	--	0.30	3.75	22.5%	12.63
Plant V	Surge	17.9	653.0	Circ	1.5	--	--	--	--	0.45	5.00	31.0%	11.12
Plant BJ	Safety Relief	19.2	653.0	Axial	1.4	1.23	0.40	88.0%	0.32	--	--	--	--
Plant O	SG Inlet	26.6	620.0	--	--	--	--	--	--	--	--	--	--
Plant AB	Safety Relief	23.1	653.0	Axial	1.3	0.10	0.60	7.7%	6.00	--	--	--	--

Table A-7
Summary of Weibull Distribution Parameter Fitting Results for DMW Analysis

Fitting Method	β	θ (EDY)	Standard Error in Weibull Slope	Standard Error in Vertical Intercept (ln(EDY))
Maximum Likelihood	1.055	1547		
Linearized Least Squares	1.015	1453	0.111	0.409

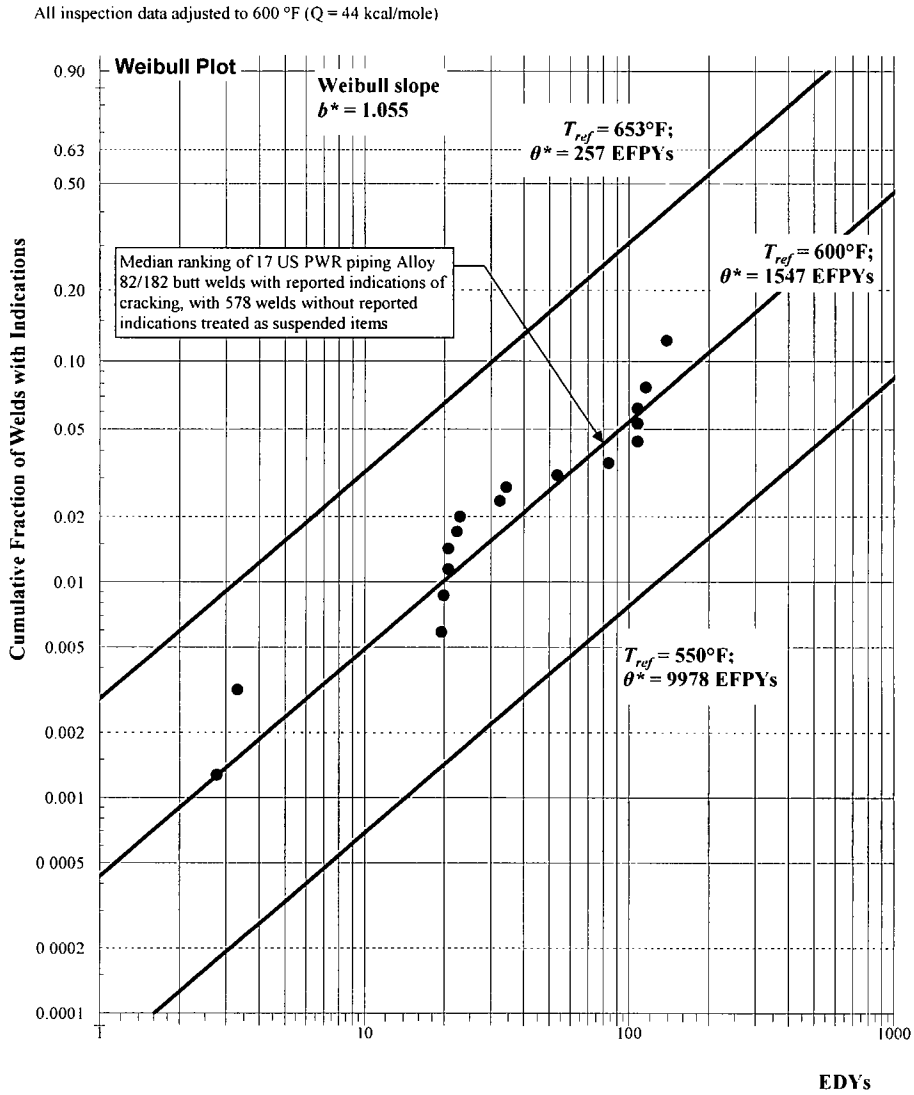

Figure A-10
Example MLE Weibull Probability Distribution for Alloy 82/182 Piping to Nozzle Butt Welds

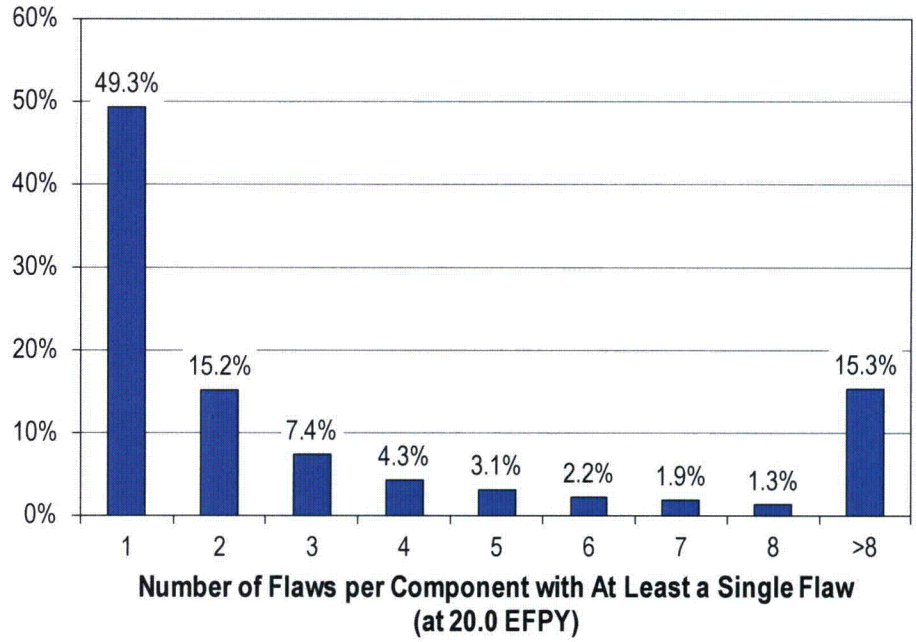

Figure A-11
Result for DM Weld Numerical Study: Distribution of Number of Flaws per Component with at Least a Single Flaw

A.8.3 Crack growth model

The set of inputs for the PWSCC propagation model is described in Table A-8 at the end of this section, including deterministic and distributed inputs. Various inputs are detailed in the following subsections.

A.8.3.1 Empirical Growth Parameters

The general flaw propagation rate equation used in this study is given in Equation [A-40]. The flaw propagation rate constant for growth in Alloy 182/82, α_{weld}, is based on MRP-263 and is taken as a deterministic input. Likewise, the stress intensity factor threshold and propagation rate stress intensity factor exponent (for growth in Alloy 182/82) are based on MRP-263 and are taken as deterministic inputs.

A.8.3.2 Growth Variation Factors

The uncertainty in the probabilistically calculated flaw propagation is principally characterized by the f_{weld} and f_{ww} parameters in the MRP-263 flaw propagation rate equations described Section A.5.3.

The f_{weld} parameter is a common factor applied to all specimens fabricated from the same weld to account for effects of the weld wire/stick heat processing and of weld fabrication. For this study, the log-normal distribution fit to the weld

factors for the set of laboratory test welds assessed in MRP-263 is used (see Figure A-12).

A "within weld factor" (f_{ww}) is included to describe the variability in flaw propagation rate for different weld specimens fabricated from the same test weld. Log-normal distributions were developed and are shown in Figure A-13 to describe the variability in f_{ww} observed for the data generated in MRP-263. The f_{ww} distribution describes the scatter in the flaw propagation rate model that remains after all effects addressed by the model are considered including the particular f_{weld} parameter calculated for each test weld.

Because there is a physical upper limit to the rate at which PWSCC crack propagation can proceed, an upper truncation limit is applied when sampling f_{weld} or f_{ww}. The f_{weld} or f_{ww} upper bound is set to the maximum of: the 95th percentile of the respective distribution and the maximum calculated f_{weld} or f_{ww}, respectively. The lower bound is imposed in a similar manner as the 5th percentile of the distribution.

Note that when an f_{ww} factor is applied in addition to the f_{weld} factor, the product of the two corresponding upper truncation limits proscribes the maximum flaw propagation rate that can be applied within the flaw propagation model. That maximum flaw propagation rate is assured to be greater than the maximum flaw propagation rate actually observed in any of the laboratory tests used to develop the f_{weld} and f_{ww} distributions when the conditions for each test are applied to the applicable flaw propagation rate equation.

A.8.3.3 Uncertainty in Temperature Effect

The temperature dependence of the flaw propagation process is modeled using a thermal activation energy. As shown in Table A-8, a normal distribution is used to describe the uncertainty in the activation energy. The standard deviation assumed corresponds to 5 kJ/mole, relative to the 130 kJ/mole mean activation energy value, and is based on engineering judgment given experience with the range of PWSCC flaw propagation activation energy values reported by various investigators for Alloy 600 wrought material.

A reference temperature of 617°F is chosen as the reference temperature for the crack growth model. The uncertainty in the activation energy accounts for the uncertainty in the temperature effect between 617°F and the operating temperature.

A.8.3.4 Correlation in Relating Flaw Initiation and Propagation

As discussed in A.5.3, it is generally accepted by PWSCC experts [21] that components that are more susceptible to PWSCC flaw initiation than other components tend to have higher flaw propagation rates than those other components. The main challenge in correlating the time to initiation and the flaw propagation rate in a probabilistic PWSCC assessment is that there is a general lack of data with which to choose an appropriate correlation coefficient. In the absence of data to select an appropriate correlation coefficient, the input

could be treated as a sensitivity parameter. The correlation coefficient was therefore set to zero for the base case analysis.

A.8.3.5 Crack Coalescence Factor

Crack coalescence modeling requires a distance threshold at which coalescence occurs. In this study, this threshold is modeled by some deterministic ratio of the maximum depth of the two cracks for which coalescence is assessed (that ratio being $1/F_{coalescence}$). For the base case result, the $F_{coalescence}$ parameter is inputted as an arbitrarily large number such that cracks must abut for coalescence to occur.

Table A-8
Summary of Inputs for DM Weld Flaw Propagation Model

Symbol	Description	Source	Units	Distrib. Parameter	Value for Base Case
Q_g	Thermal activation energy for PWSCC flaw propagation	Q values from MRP-263; stdev based on judgment; see Note 1	kJ/mole	type	Normal
				mean	130
				stdev	5
				min	100
				max	160
				deterministic	130
T	Component operating temperature	See component-specific tables in this report			
f_{weld}	Weld factor: common factor applied to all specimens fabricated from the same weld to account for weld wire/stick heat processing and for weld fabrication	By definition, the median within weld factor is one; Distributions from fits shown in figures of this document	Nondim	type	Log-Normal
				linear μ	1.13
				log-norm μ	0.00
				log-norm σ	0.4895
				min	0.440
				max	2.24
f_{ww}	Within Weld factor: factor accounting for the variability in crack growth rate for different specimens fabricated from the same weld	By definition, the median within weld factor is one; Distributions from fits shown in figures of this document	Nondim	type	Log-Normal
				linear μ	1.07
				log-norm μ	0.00
				log-norm σ	0.3742
				min	0.355
				max	2.04
ρ_{weld}	Correlation coefficient for PWSCC initiation and propagation of all cracks in weld	No basis for selection of non-zero base case value	Nondim		0.00
ρ_{ww}	Correlation coefficient for PWSCC initiation and propagation of specifc crack	No basis for selection of non-zero base case value	Nondim		0.00
α	Flaw propagation rate equation power law constant	Table F-2 of MRP-263	(m/s)/ $(MPa\text{-}m^{0.5})^{1.6}$		2.01E-12
b	Flaw propagation rate equation power law exponent	Best fit per MRP-263	Nondim		1.6
K_{Ith}	K_I Stress intensity factor threshold	MRP-263	$MPa\text{-}m^{0.5}$		0
$T_{ref,g}$	Absolute reference temperature to normalize PWSCC flaw propagation data	MRP-263	°F		617
Δt	Time step size for crack increment	1 month assumed	yr		1/12
$F_{coalescence}$	Reciprocal of the ratio of maximum crack depth that is used to evaluate the critical separation distance for coalescence	Set arbitrarily large such that coalescence occurs only once two cracks overlap	Nondim		Arbitrarily large value
K_{90}	Stress intensity factor at deepest point on crack front	SIF model	$MPa\text{-}m^{0.5}$		calculated by SIF models
K_0	Stress intensity factor at surface point on crack front	SIF model	$MPa\text{-}m^{0.5}$		calculated by SIF models

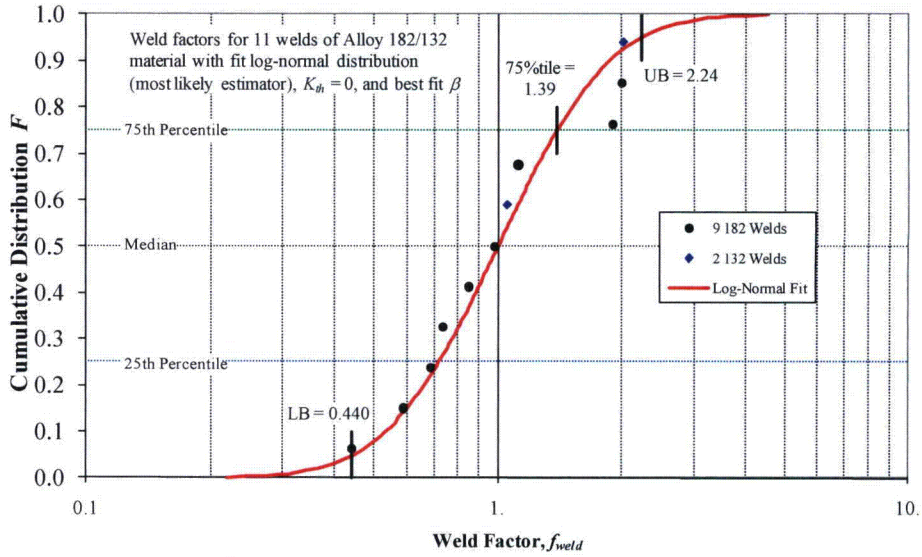

Figure A-12
MRP-263 Weld Factor f_{weld} Distribution [12] with Log-Normal Fit for Alloy 182/132

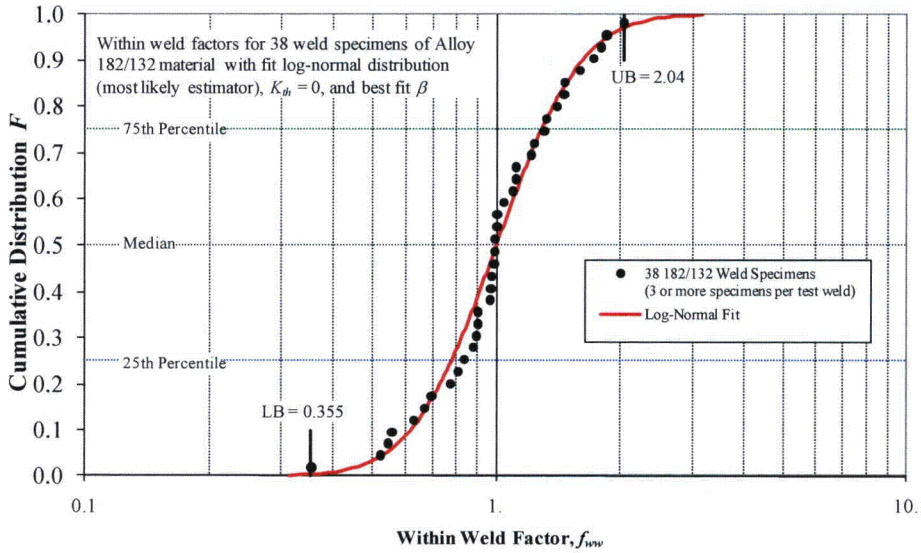

Figure A-13
MRP-263 Within Weld Factor f_{ww} Distribution [12] with Log-Normal Fit for Alloy 182/132

A.8.4 Flaw detection model

The set of inputs for the flaw examination models is described in Table A-9 at the end of this section, including deterministic and distributed inputs. Various inputs are detailed in the following subsections.

A.8.4.1 Examination Scheduling

As mentioned in the modeling section, UT inspection scheduling prior to peening for DM welds is based on ASME Code Case N-770-1 [16]. Accordingly, a UT inspection is simulated once every three cycles for the RVON and once every four cycles for the RCP nozzle. The first PDI qualified UT inspection is modeled as occurring in Fall 2009 (the end of the 14th simulated cycle) for the RVON and Spring 2010 (the end of the 15th cycle) for the RCP inlet/outlet. These dates correspond with the units that were used to develop the operating timeline, temperature, and geometry inputs discussed in Section A.8.1.

In cases where peening is scheduled, the follow-up and in-service inspection intervals are varied to generate comparative results. The follow-up interval is varied between 1, 2, or 3 cycles. The in-service inspection interval is varied from 3 cycles (same as the unrelieved ISI) to the plant lifetime for the RPV outlet and from 4 cycles to the plant lifetime for the RCP inlet/outlet.

For the baseline set of results, ET inspections are not simulated during the pre-peening inspection. This scenario is included as a sensitivity.

A.8.4.2 UT Probability of Detection

The UT POD model for DM welds is described by Equation [A-44]. Based on the study of UT qualification data published in MRP-262 Revision 1 [17], the uncertainty of the detection model parameters, $\beta 1$ and $\beta 2$, can be accurately captured using a bivariate normal distribution. The distribution parameters for POD of DM weld cracking on RVONs from this study are given in Table A-9. Note that these parameters are also applied for the RCP nozzle case given that the RCP nozzle has a geometry similar to a RVON.

As discussed in the modeling section, the study used to derive the UT POD curve discussed above did not include axial cracks. Experience indicates a decreased capability to detect axial cracks relative to circumferential cracks using UT. Accordingly, a deterministic reduction factor of 0.8 is conservatively applied to the POD predicted by the model from [17] in order to model detection of axial flaws by UT. The factor of 0.8 is conservative given the 80% detection rate specified by Appendix VIII of Section XI for qualification of UT procedures and personnel.

A correlation coefficient relating the results of the next inspection to the results of the previous inspection can be included to take into account the increasing likelihood of non-detection if a crack has already been missed in a previous inspection. Because this value has not been experimentally determined, a modest correlation coefficient of 0.5 is used for the base case input.

A.8.4.3 ET Probability of Detection

The probabilistic ET POD model is described by Equations [A-45] and [A-46]. The ET POD curve parameters were loosely based on vendor data provided by

Mitsubishi Nuclear Engineering Services and Hitachi-GE, as well as EPRI's eddy current Examination Technique Specification Sheets:

- Mitsubishi reported the ability to detect cracks based on their location. For RV inlet/outlet butt welds, cracks 0.5 mm or deeper were detected. For BMN inner surfaces, cracks 0.4 mm or deeper were detected. For BMN J-weld surfaces, cracks 0.9 mm or deeper were detected [29]. These detection depths correspond to a signal-to-noise ratio of 2.
- Hitachi-GE reported the ability to detect flaws with depths greater than 0.5 mm and lengths greater than 3.3 mm on BMNs [25].
- EPRI's eddy current Examination Technique Specification Sheets indicate detectability of cracks with depths 0.7 mm or greater [26].

As discussed early, the ET inspection model is generated from upper and lower POD curves which each represent a two standard deviation offset from the mean POD curve. The upper bound (favorable) curve was chosen such that there is a 50% POD for cracks 0.5 mm deep and a 75% POD for cracks 0.7 mm deep. The lower bound (unfavorable) curve was chosen such that there is a 50% POD for cracks 1.0 mm deep and a 75% POD for cracks 1.2 mm deep. Finally, a maximum POD of 95% is used to account for human/equipment error or other factors. The lower, upper, and mean POD curves are shown in Figure A-14.

In addition to the POD curve as a function of crack depth, experience indicates that there exists a minimum crack length below which cracks are very difficult to detect by ET. A deterministic input of 2 mm was selected for this length.

Table A-9
Summary of Inputs for DM Weld Examination Model

Symbol	Description	Source	Units	Distrib. Parameter	Value for Base Case
β_1	POD model for 0th order logistic equation parameter for Category B1 components: RV Inlet and Outlet	Table 12-3 of MRP-262	Nondim	type	Normal
				mean	3.2440
				stdev	0.5490
				deterministic	3.2440
β_2	POD model for 1st order logistic equation parameter for Category B1 components: RV Inlet and Outlet	Table 12-3 of MRP-262	Nondim	type	Normal
				mean	1.06
				stdev	1.32
				deterministic	1.06
ρ_β	Correlation coefficient for Category B1 component POD model parameters	MRP-262 Wald Model Results in Appendix B	Nondim		-0.86980
$f_{UT,axial}$	Reduction factor applied to POD predicted from circumferential crack detection data	Engineering judgment	Nondim		0.80
$(a_{U,1,ET}, p_{U,1,ET})$	First defined coordinate for favorable ET POD curve	Engineering judgment, NDE experts, literature	(mm,Nondim)		(0.5,0.5)
$(a_{U,2,ET}, p_{U,2,ET})$	Second defined coordinate for favorable ET POD curve	Engineering judgment, NDE experts, literature	(mm,Nondim)		(0.7,0.75)
$(a_{L,1,ET}, p_{L,1,ET})$	First defined coordinate for unfavorable ET POD curve	Engineering judgment, NDE experts, literature	(mm,Nondim)		(1.0,0.5)
$(a_{L,2,ET}, p_{L,2,ET})$	Second defined coordinate for unfavorable ET POD curve	Engineering judgment, NDE experts, literature	(mm,Nondim)		(1.2,0.75)
$p_{max,ET}$	Maximum probability of detection for ET inspection	Engineering judgmet	Nondim		0.95
$c_{min,ET}$	Minimum detectable crack length	Engineering judgment, NDE experts, literature	mm		2.00
ρ_{insp}	Correlation coefficient for successive UT inspections	Engineering judgment	Nondim		0.50

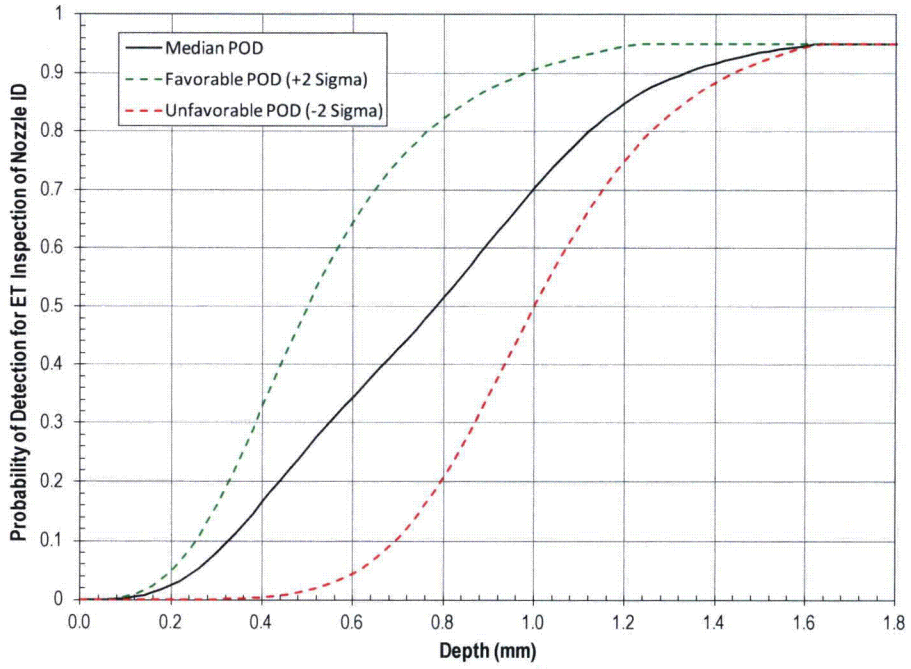

Figure A-14
Assumed POD Curve for ET Inspection of Nozzle ID

A.8.5 Effect of peening on residual stress

The set of inputs related to peening considerations is described in Table A-10 at the end of this section, including deterministic and distributed inputs. Various inputs are detailed in the following subsections.

A.8.5.1 Peening Application Scheduling

For both the hot and cold leg DM weld components, the peening application is scheduled for the outage coinciding with the second UT inspection. This reflects the fact that the first PDI qualified UT inspection of DM welds occurred recently (e.g., 2009 and 2010) and that peening is assumed to be performed as soon as possible, but in the most economical fashion.

Given the first inspection times and inspection intervals defined in Section A.8.1.2, the time of peening application for the hot leg component is EOC 17 and the time of peening application for the cold leg component is EOC 19.

A.8.5.2 Post-Peening Residual Stresses

The parameterized model for post-peening residual stress profiles are described in Equations [A-17] through [A-21].

Uncertainty in the peening stresses is incorporated by using distributions for the magnitude of the compressive surface stress and the depth of the peening layer. These distributions were determined based on data and qualitative information

provided by peening vendors (e.g., Hitachi-GE, Toshiba, MHI) as documented in MRP-267 Revision 1 [4]. In general, the vendor-supplied data included measured stresses, often in two orthogonal directions, at various depths between the peened surface and approximately 1-2 mm. Other information, including the peening type, the specimen material, specimen geometry, and specimen stress state prior to peening, was generally available for each measured stress profile. This data is summarized in Table A-11 and Table A-12, for specimens peened by ULP and WJP, respectively[12].

For each measured stress profile, measurements were available at between 5 and 20 depths. A linear equation was fit to this data for each profile and the resulting fit was used to approximate the surface stress and the peening depth, as demonstrated in Figure A-15. Table A-11 and Table A-12 give these approximated characteristics, as well as the coefficient of determination value, for each linear fit.

The sample mean and standard deviation for surface stress, calculated across the 66 ULP and WJP stress profiles, are -544 and 181 MPa (-78.9 ksi and 26.3 ksi). A normal distribution with this sample mean and standard deviation is assumed for the initial surface stress of the DM weld ID after peening. An upper truncation limit of 0 MPa is used to reflect the assumption that the residual surface stress is always compressive after peening (across the 66 stress profiles, the minimum surface stress magnitude belonged to a specimen with an approximated surface stress of -239 MPa or -34.7 ksi).

The peening compressive residual stress depth for the DM weld ID is also modeled with a normal distribution. This distribution is given a mean of 1.0 mm. This value is supported by the data discussed above. A standard deviation of 0.25 is used to account for variation in the application characteristics. While the data indicates a larger standard deviation, this is due in large part to the error in the linear fit. Furthermore, the data spans many different geometries and application degrees of freedom, whereas the application on in-service DM welds is expected to be more controlled. The non-realistic case of negative penetration depth is prevented by using a lower truncation bound of 0.0 mm.

To define the transition from the compressive surface layer to the pre-peening stress profile, two characteristic lengths are required (as detailed in Section A.3.3 and Figure A-4). The first length, $x_{2,PPRS}$, defines the distance from the peened surface to the point where the pre-peening WRS profile is regained. The second length, $x_{3,PPRS}$, defines the distance from the peened surface to the point where the post-peening, stress-balanced WRS profile is regained. These lengths are defined with deterministic ratios:

---

[12] Measured stress profiles from stainless steel specimens were included in the set of data that informed modeling and inputs for peened components. The key characteristics of these stress profiles (e.g., stress at the surface; penetration depth) were not found to be statistically different from those of Alloy 600 and its weld metals. For instance, the mean and standard deviation of post-peening surface stress across 51 Alloy 600/182/132 samples were -544 and 183 MPa; these same metrics across 15 stainless steel samples were -547 and 181 MPa.

$$x_{3,PPRS} = f_{1,PPRS} x_{1,PPRS}$$
$$x_{2,PPRS} = x_{1,PPRS} + f_{2,PPRS}(x_{3,PPRS} - x_{1,PPRS}) \quad [A\text{-}50]$$

These ratios were defined based on engineering judgment as little measured data was available beyond 1-2 mm from the peened surface. Their values are given in Table A-8.

A.8.5.3 Thermal and Load Cycling

To estimate the stress relaxation occurring in a peened component over a plant lifespan, experimental data monitoring residual surface stress measurements on a peened surface as a function of time were analyzed. Specifically, measurements were available for three Alloy 182 specimens treated with WJP by Hitachi-GE [4]. These data are shown in Figure A-16.

To accelerate the stress relaxation, the experiments were performed at a temperature of 842°F (450°C) for 1000 hr, which is much higher than typical component temperatures during operation. This temperature and duration were converted to an equivalent operating time at 620°F (327°C) using an Arrhenius relationship with an activation energy of 188 kJ/mol, which corresponds to the lower bound of an activation energy range for creep of Alloy 600 in primary water determined by Was et al. [27]. This results in a total equivalent operating time of approximately 69 EFPY at 620°F (327°C). So, the thermal stress relaxation fraction for a plant lifetime, f_{relax}, could be determined from the average ratio of residual stress at the end of the experiment to the residual stress just after peening. This value is applied immediately to the sampled initial peening surface stress discussed in the previous subsection. In the Hitachi-GE data, the majority of the residual stress relaxation was observed within 1 h (equivalent to approximately 25 days at 620°F), which justifies the application of the stress relaxation factor immediately after peening.

The reduction in peening compressive residual stress level assumed in the probabilistic calculations is considered to conservatively address the effects of thermal relaxation due to prolonged elevated temperature exposure, as well as due to load cycling (i.e., stress shakedown). The load cycling testing performed by NRI for EPRI [4] (on samples peened by all the candidate methods considered in this report) was performed in combination with exposure to a temperature of 300°C for a total time of about 2000 hours. The other stress relaxation testing described in MRP-267 Revision 1 [4] indicated that the majority of the stress relaxation occurs early in the elevated temperature tests performed. Thus, the NRI tests are considered to adequately represent the combined effects of thermal relaxation and load cycling. Finally, the probabilistic inputs encompass the level of stress relaxation exhibited in the NRI tests.

A.8.5.4 Effect of Peening on Growth

For the baseline results, growth of cracks is simulated without consideration for crack closure. This effect is considered as a sensitivity case.

Also for the baseline results, full credit is given to growth of the length of a crack under the peening surface. As discussed in Section A.5.5, this is done by using the "balloon" growth approximation – neglecting peening stresses for the calculation of length growth. The "balloon" growth approximation is lifted for a sensitivity study.

Table A-10
Summary of Peening-Specific Inputs for DM Weld Model

Symbol	Description	Source	Units	Distrib. Parameter	Value for Base Case
	Outage of peening application for hot leg RVON	Scheduled at next outage coinciding with a UT inspection	EOC		17
	Outage of peening application for cold leg RVON	Scheduled at next outage coinciding with a UT inspection	EOC		19
	Number of cycles between peening application and follow-up	MRP-336	# cycles		varied from 1,2,3
	Inspection frequency after peening for hot leg component	MRP-336	(# cycles)$^{-1}$		varied from 3,6,12,∞
	Inspection frequency after peening for hot leg component	MRP-336	(# cycles)$^{-1}$		varied from 4,6,12,∞
$\sigma_{0,PPRS}(t=0)$	Initial peening stress on applied surface	Vendor-supplied data for fiber laser- and water jet-peened surfaces	MPa	type	Normal
				mean	-544
				stdev	181
				min	-1000
				max	0
$x_{1,PPRS}$	Depth from surface where peening residual stress crosses zero	Information for vendors and vendor-supplied data for fiber laser- and water jet- peened surfaces	mm	type	Normal
				mean	1.00
				stdev	0.25
				min	0.00
				max	2.50
$f_{1,PPRS}$	Ratio of minimally-affected depth to penetration depth	Engineering judgment	Nondim		2.00
$f_{2,PPRS}$	Fraction of depth between penetration depth and minimally-affected depth where peening results in no net effect	Engineering judgment	Nondim		0.70
f_{relax}	Estimated reduction factor of peening residual stresses after approximately 60 years at operational temperatures	Hitatchi experimental data for relaxation of Alloy 182 specimans after WJP	Nondim		0.746
	Flag indicating if crack growth will be predicted considering the effect of crack closure	Crack closure effects are neglected for base case	Logical		False
	Flag indicating if cracks may growth in length without the effect of peening stresses	Cracks are allowed to grow in length without effect of peening to approximate sub-surface balloon growth of crack	Logical		True

Table A-11
Summary of Peening Data (ULP)

Speciman Material	Specimen Geometry	Pre-Peening Surface Stress (MPa)	Approximated Post-Peening Surface Stress (MPa)	Approximated Penetration Depth (mm)	R^2 of Linear Fit to Stress Profile
304SS	Rectangular Plate	-295	-692	0.94	0.837
304SS	Rectangular Plate	200	-897	0.61	0.928
304SS	Rectangular Plate	266	-592	1.11	0.954
304SS	Welded Plate	N/A	-555	1.05	0.822
304SS	Welded Plate	N/A	-373	1.37	0.792
316L SS	Rectangular Plate	-305	-847	0.83	0.802
316L SS	Rectangular Plate	185	-742	0.96	0.789
316L SS	Rectangular Plate	N/A	-420	1.03	0.869
316L SS	Rectangular Plate	N/A	-660	0.94	0.739
Alloy 132	Rectangular Plate	-53	-583	1.20	0.758
Alloy 132	Rectangular Plate	482	-762	1.16	0.851
Alloy 182	Rectangular Plate	-160	-687	1.14	0.840
Alloy 182	Rectangular Plate	485	-1006	0.90	0.916
Alloy 600	BMN-Sized Pipe ID	-400	-560	1.00	0.662
Alloy 600	BMN-Sized Pipe ID	-200	-500	1.14	0.701
Alloy 600	BMN-Sized Pipe OD	-400	-806	0.49	0.825
Alloy 600	BMN-Sized Pipe OD	-200	-375	0.83	0.730
Alloy 600	Rectangular Plate	-2	-370	1.01	0.879
Alloy 600	Rectangular Plate	24	-575	0.95	0.965
Alloy 600	Rectangular Plate	37	-653	1.13	0.852
Alloy 600	Rectangular Plate	440	-875	1.03	0.839
Alloy 600	Rectangular Plate	N/A	-851	1.52	0.900
Alloy 600	Rectangular Plate	N/A	-339	0.92	0.888
Alloy 600	Rectangular Plate	N/A	-447	0.88	0.921
Alloy 600	Welded Plate	-550	-676	1.00	0.748
Alloy 600	Welded Plate	-550	-510	1.70	0.529
Alloy 600	Welded Plate	-540	-783	0.96	0.813
Alloy 600	Welded Plate	-540	-767	1.82	0.671
Alloy 600	Welded Plate	-483	-887	0.35	0.994
Alloy 600	Welded Plate	-483	-774	0.78	0.786
Alloy 600	Welded Plate	-207	-604	1.01	0.787
Alloy 600	Welded Plate	-207	-603	1.00	0.763
Alloy 600	Welded Plate	-205	-546	1.43	0.736
Alloy 600	Welded Plate	-205	-492	1.68	0.864
Alloy 600	Welded Plate	-47	-737	0.67	0.996
Alloy 600	Welded Plate	-47	-779	0.42	0.999
Alloy 600	Welded Plate	61	-467	1.95	0.584
Alloy 600	Welded Plate	61	-554	1.18	0.802
Alloy 600	Welded Plate	345	-536	1.00	0.836
Alloy 600	Welded Plate	350	-605	1.09	0.976
Alloy 600	Welded Plate	350	-433	1.24	0.781
Alloy 600	Welded Plate	430	-381	1.00	0.896

Table A-12
Summary of Peening Data (WJP)

Speciman Material	Specimen Geometry	Pre-Peening Surface Stress (MPa)	Approximated Post-Peening Surface Stress (MPa)	Approximated Penetration Depth (mm)	R^2 of Linear Fit to Stress Profile
304SS	Rectangular Plate	241.325	-415	0.82	0.933
304SS	Rectangular Plate	241.325	-353	0.70	0.666
304SS	Rectangular Plate	517.125	-408	0.66	0.786
316L SS	Rectangular Plate	489.545	-443	0.91	0.868
316L SS	Rectangular Plate	489.545	-409	0.68	0.792
316L SS	Rectangular Plate	517.125	-399	1.03	0.709
Alloy 182	Rectangular Plate	434.385	-527	0.60	0.751
Alloy 600	BMN Mock Up ID	70	-316	0.51	0.879
Alloy 600	BMN Mock Up ID	256	-369	0.79	0.903
Alloy 600	BMN Mock Up ID	406	-293	0.52	0.984
Alloy 600	BMN Mock Up ID	460	-365	0.55	0.946
Alloy 600	BMN Mock Up OD	N/A	-461	2.84	0.909
Alloy 600	BMN Mock Up OD	N/A	-394	2.87	0.859
Alloy 600	BMN Mock Up OD	N/A	-352	1.57	0.980
Alloy 600	BMN Mock Up OD	N/A	-284	2.66	0.553
Alloy 600	BMN-Sized Pipe ID	503.335	-509	0.61	0.805
Alloy 600	BMN-Sized Pipe ID	510.23	-390	0.75	0.392
Alloy 600	Rectangular Plate	268.905	-349	0.66	0.685
Alloy 600	Rectangular Plate	510.23	-492	0.95	0.838
Alloy 600	Rectangular Plate	510.23	-379	1.02	0.668
Alloy 600	Rectangular Plate	N/A	-616	0.93	0.778
Alloy 600	Rectangular Plate	N/A	-549	1.84	0.938
Alloy 600	Welded Plate	562	-239	4.14	0.326
Alloy 600	Welded Plate	873	-331	1.36	0.743

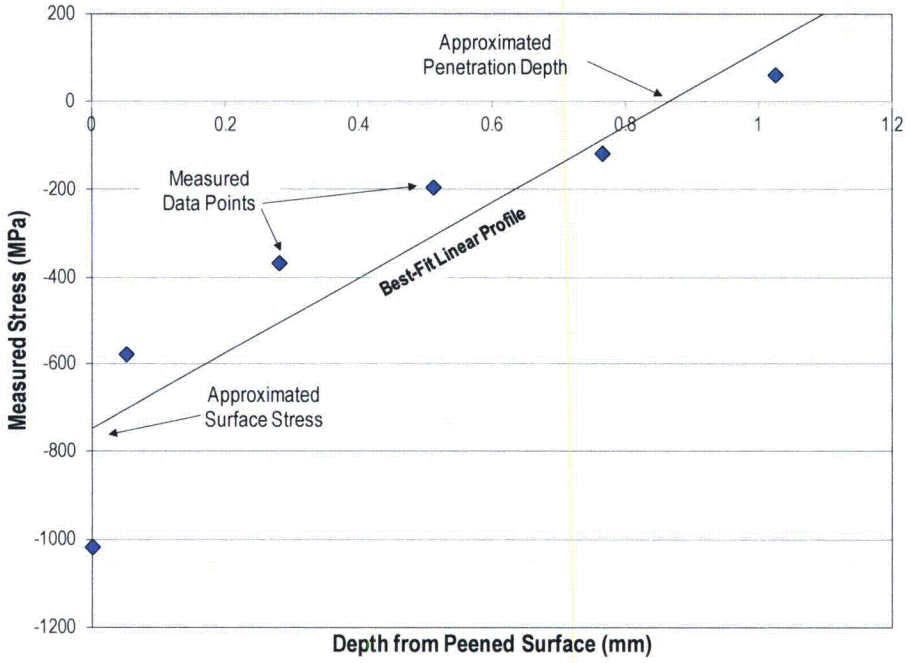

Figure A-15
Example Linear Fit to Stress Profile Data

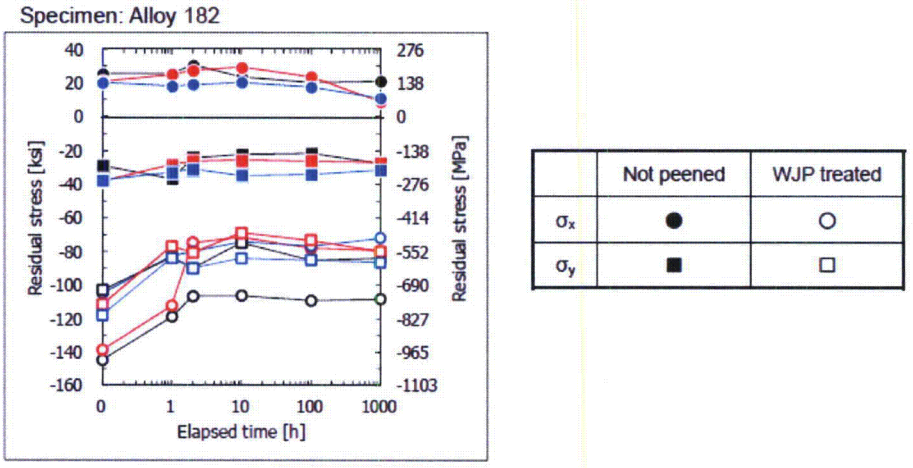

Figure A-16
Experimental Data used to Estimate Thermal Residual Stress Relaxation Factor

A.9 Results of probabilistic cases

This section presents results generated using the integrated probabilistic model described in Sections A.2 through A.6, with particular focus on the prediction of the leakage criterion described in Section A.7. Using the inputs described in Section A.8, this section presents predictions for hot and cold leg DM weld

components without peening mitigation (Section A.9.1) and with peening mitigation (Section A.9.2).

Section A.9.3 presents the results of sensitivity studies wherein one or more inputs or modeling methodologies were varied from those described in Sections A.2 through A.8. The aim of these sensitivity studies is to demonstrate the relative change in the predicted leakage risk for a DM weld component when an input or modeling assumption is varied.

Because various assumptions and simplifications were involved in the development of the integrated probabilistic model, the magnitudes of the predicted risks for any given case may include a substantial bias error. Accordingly, the more vital conclusions are drawn from the relative differences between risks predicted for different cases (e.g., between the risks predicted for one peening schedule vs. those predicted with a different peening schedule).

A.9.1 Results for the unmitigated case

Using the inputs specified in Section A.8, predictions were made for the hot and cold leg DM weld components without any peening mitigations; leakage probability vs. time predictions are given in Figure A-17 and Figure A-18, respectively. For these cases, inspections were scheduled based on N-770-1 for unmitigated components.

For reference, the hypothetical time of peening is shown on these plots. As discussed in the inputs section, this time of peening has been set to coincide with the next UT inspection scheduled after present day. Between the hypothetical time of peening and 60 calendar years (55.2 EFPY), the model predicts a cumulative probability of leakage of 2.6E-02 for the hot leg component and 7.6E-04 for the cold leg component. These values will be important for assessing the performance of peening with respect to leakage mitigation in the following section.

A.9.2 Results with peening mitigation

As discussed previously, a follow-up inspection is expected to be conducted either one, two, or three cycles after peening, and after the follow-up inspection, a new in-service inspection interval is expected to be utilized through the end of plant life. Various combinations of follow-up inspection time and in-service inspection frequency were used to make leakage risk predictions after peening. These results are summarized in Figure A-19 and Figure A-20 for the hot and cold leg components, respectively. It is emphasized that a surface inspection is not modeled at the pre-peening inspection for these results. This is instead addressed as a sensitivity case.

For both the hot and cold DM weld components, the predicted likelihood of cracks existing after the pre-peening inspection is very low; less than 3E-04.

For the RVON, the program predicts that the cumulative probability of leakage after peening is reduced by a factor between 120 and 200, (compared to cumulative leakage probabilities on same span of time for an unmitigated RVON). While there is some small trend with respect to follow-up time, in general the degree of improvement is not significantly influenced by the follow-up time or the ISI frequency. The former is the result of the fact that most of the cracks that go undetected at the pre-peening inspection are small, and accordingly grow slowly after peening (see deterministic calculations that demonstrate this in Section 5.2); the latter is a result of the fact that nearly all cracks are detected during the pre-peening or follow-up inspection and no new cracks are expected to initiate after peening.

For the RCP nozzle, the program predicts that the cumulative probability of leakage after peening is reduced by a factor between 9 and 12, (compared to cumulative leakage probabilities on same span of time for an unmitigated RCP nozzle). This degree of improvement is smaller than that predicted for the hot leg component because the inspection schedule for an unmitigated cold leg component conservatively takes little credit for its reduced temperature in comparison to that for hot-leg locations.

For both the hot and cold DM weld components, the probability of leaking after the follow-up inspection is very low; less than 7E-05 in all cases. Figure A-21 demonstrates the decaying nature of leakage probability vs. time after peening, for both the cold and hot components with relieved UT inspection intervals. This may be important for establishing post-peening BMV scheduling.

A.9.3 Results for sensitivity cases

Various sensitivity studies were conducted with the DM weld probabilistic model in order to demonstrate the relative change in the predicted results given one or more changes to modeling or input assumptions. Each sensitivity case has been classified as either a Model Sensitivity (in which an approximated input or model characteristic is varied) or an Inspection Sensitivity (in which a controllable inspection option is varied). These sensitivity cases are described in Table A-13 and Table A-14.

The relative changes in the predicted cumulative probability of leakage after the hypothetical time of peening, for all sensitivity studies, are given in Figure A-22 (for cases in which peening was applied) and Figure A-23 (for cases in which peening was not applied). Results are given for the RVON, instead of the RCP nozzle, because these components were predicted to have a higher general probability of leakage.

A handful of intriguing cases have been selected for a more detailed discussion below:

DMW Model Sensitivity Cases 1 and 2 – NB-3600 [28] Bending Loads

To study the effect of worst-case bending loads on leakage, the high and extreme loads calculated with NB-3600 [28] equations were applied to RVON in DMW Model Sensitivity Cases 1a and 2a, respectively.

The high bending load calculated using NB-3600 equations is very nearly the same load used to produce base case results and as expected the results of the base case and Case 1 are similar.

The extreme bending load calculated using NB-3600 equations is approximately 90% larger than the load used in the base case. While this resulted in a modest increase (13%) in the probability of the leakage for the unmitigated component, it counter-intuitively reduced the probability of leakage for the peened component. This is partially due to the fact that the higher bending results in faster crack growth prior to peening, and thus higher probabilities of detection at the pre-peening inspection. However, it is partially due to a modeling artifact: as the bending load increases, the maximum stress used in Equation [A-34] increases relative to stresses at other locations resulting in a more significant initiation time stress adjustment at these other locations. This is especially significant for the initiation of axial cracks whose stress does not increase with the bending load.

To address this effect (in Model Sensitivity Cases 1b and 2b), a reduction factor is applied to t_1 of the first crack initiation time model.

$$t_i' = f_{adjust} t_i \qquad \text{[A-51]}$$

This results in earlier first crack initiation to counteract the reduction in the mean arrival time of multiple crack initiation. The reduction factor is calculated to normalize the initiation times of the extreme bending case:

$$f_{adjust} = \left(\frac{\sigma_{surf,base}}{\sigma_{surf,extreme}} \right)^n \qquad \text{[A-52]}$$

where $\sigma_{surf,base}$ and $\sigma_{surf,extreme}$ are the nominal surface stresses at the point of maximum bending for the base case and the extreme loading case, respectively.

With this adjustment, the probability of leakage increased by 145%for the unmitigated component and increased by 27% for the peened component. This suggests that the faster rate of growth due to the larger bending load outweighs the larger POD at the pre-peening inspection.

DMW Model Sensitivity Case 4: Time-Dependent Residual Stress Relaxation

As an alternative to the instantaneous peening stress relaxation model used for the base case, DMW Model Sensitivity Case 4 explored the use of a time-dependent stress relaxation model.

Given only a small set of experimental stress relaxation data for Alloy 182 supplied by peening vendors, a simple exponential model was deemed appropriate for this study:

$$\sigma_{PPRS,d}\left(x,\Delta t_{peen}\right)=\sigma_{PPRS,d}\left(x,\Delta t=0\right)\cdot\exp[-m\cdot\Delta t_{peen}] \qquad \text{[A-53]}$$

where Δt_{peen} is the time elapsed since peening (in EFPYs) and m is the empirical stress relaxation exponent. It is noted that this approach relaxes both the peening and welding residual stresses, whereas the method used in the base case conservatively relaxed only peening stresses. Welding residual stresses are not relaxed until after the time of peening, resulting in higher likelihood of crack formation and growth prior to peening.

After linearizing the exponential model, a best-fit value of the stress relaxation exponent was calculated with linear least squares regression. A value of 4.71E-03 $EFPY^{-1}$ was estimated. This results in a stress relaxation vs. time that is nearly linear between 0 and 60 years (55 EFPY).

As demonstrated in Figure A-22, the relative change caused by applying this model was negligible. This may be the result of competing effects (e.g., slower relaxation of compressive peening stresses vs. the use of welding residual stress relaxation). More likely, it demonstrates insensitivity in the leakage risk to the exact manner in which residual stress relaxation is modeled.

DMW Model Sensitivity Case 6: Correlation of Initiation and Growth

DMW Model Sensitivity Case 6 explored the generally accepted tendency for cracks that initiate earlier to grow faster; specifically it explored this tendency's impact on the leakage probability predictions. This tendency is implemented by adding a negative correlation between the time of first crack initiation on DM weld component, t_{ref}, and the weld-to-weld variation factor, f_{weld}, as well as between each multiple crack initiation time, $t_{ref,i}$, and the sampled within-weld variation, $f_{ww,i}$, for each crack. Erring on the side of simplicity, the base case used zero correlation because it is difficult to quantify the proper correlation coefficient. This case uses a medium/strong (-0.8) correlation coefficient for the correlations described above.

The results shown in Figure A-22 and Figure A-23 demonstrate the competing effects of crack growth rate and POD. For the peened component, adding correlation results in a 56% decrease in the probability of leakage after peening because it causes generally larger cracks at the time of the pre-peening inspection which fosters detection before the relieved inspection scheduled. However, for

the unmitigated component, adding correlation results in a 33% increase in probability of leakage because cracks that initiate during the lifetime of a DM weld component are considered early (for the corresponding chemical and material conditions) and thus grow faster.

DMW Model Sensitivity Case 8: Reduced Initial Crack Depth

The base case inputs used to make predictions for the RVON assumed an initial crack depth between 2.5%tw (1.7 mm) and 10%tw (7 mm). In reality, the initiation depth of PWSCC can be on the micro- or nano-scale, arising from manufacturing processes, other forms of corrosion, cavitation, etc. The rationale behind selecting a much larger initiation depth is that the initiation time model is based on data for detected cracks, and so it does not account for micro- or nano-scale cracks, of which there are likely many more incidences. Furthermore, the prediction of crack growth rate with the methods presented in the modeling section is compromised as the depth of the crack to be analyzed becomes smaller than approximately 0.1 mm.

Because of the importance of detection during the pre-peening and follow-up inspections, it may be non-conservative to assume cracks with large initial depths. Such cracks may more easily be detected at the pre-peening or follow-up inspections, resulting in less cracks active during the post-peening ISI schedule. DMW Model Sensitivity Case 8 assessed this possibility by using an initial crack depth distribution with a median depth 10 times less than that used for the base case, resulting in an initial crack depth approximately between 0.25%tw (0.2 mm) and 1%tw (0.7 mm). (For the nominal surface stress on a DM weld component, the stress intensity factor for a 0.2 mm crack is ~11 MPa-$\sqrt{m}$ (~10 ksi-$\sqrt{in}$), which is slightly below the crack depths used to generate the crack growth rate curve presented in Section A.5.3).

As anticipated, the smaller crack depth resulted in an increase in the probability of leakage after peening (52% larger relative to the base case) while it resulted in a slight decrease in the probability of leakage of an unmitigated component.

DMW Model Sensitivity Case 9: Earlier Initiation of First PWSCC

DMW Model Sensitivity Case 9 explored the effect of shifting the initiation time model such that initiations are predicted earlier in general. This provides an alternative approach to accounting for the fact that the initiation model used for the base case was fit to data for detected cracks; hypothetically, if undetected cracks could be included to fit the initiation model, the initiation time distribution would be shifted toward earlier times. Conservatively, the parameter t_1 of the first crack initiation model, which quantifies the time at which 1% of DM weld components are expected to initiate PWSCC, was reduced by a factor 5 for this sensitivity case.

As shown in Figure A-22 and Figure A-23, this increased the probability of leakage after the hypothetical time of peening by a factor of approximately five, for both the peened and unmitigated component. It is noted that probability of leakage for an RVON, predicted at present day, for this sensitivity case, was

approximately 10%. This is a higher probability than indicated by the incidence rate in US PWRs.

DMW Inspection Sensitivity Case 2: No Pre-Peening Inspection

The base case included a volumetric (UT) inspection during the pre-peening examination. Along with the follow-up inspection, this inspection is key for detecting significant cracks before entering the relieved inspection schedule. DMW Inspection Sensitivity Case 2 aimed to demonstrate this importance by comparing leakage risks with and without the pre-peening volumetric inspection.

When the pre-peening volumetric inspection was forgone, the probability of leakage after peening was predicted to increase by more than 10 times relative to the base case.

DMW Inspection Sensitivity Case 3: Surface Inspection Performed During Pre-Peening Inspection

The base case did not include a surface (ET) inspection during the pre-peening examination. Even without surface inspection, peened DM welds operating with relieved inspection intervals were predicted to have lower probabilities of leakage compared to unmitigated DM welds operating with the currently stipulated inspection interval. DMW Inspection Sensitivity Case 3 explored what further risk improvement might be anticipated if a surface inspection were to be scheduled during the pre-peening inspection.

The probability of leakage was predicted to be reduced by 93% when surface inspection was included during the pre-peening inspection, instead of solely a volumetric inspection. This large reduction was expected. Not only does the surface inspection provide a second, independent inspection of all potential crack sites, but it is generally more effective for small-depth cracks that may be missed by volumetric inspection.

Table A-13
Description of Model Sensitivity Cases for DM Weld Probabilistic Model

Category	Case No.	Model Sensitivity Case		
		Parameter	***Base Case***	***New Value(s)***
Base	0	Base Case: *See table of base case inputs*		
Sensitivity	1a	Load Module Bending Stress *Increase bending load per NB-3600 Eq.9*	M_{NTEy}=4519.4 MPa	M_{NTEy}=4292.7 MPa
	1b	Load Module Bending Stress *Increase bending load per NB-3600 Eq.9 with tref offset*	*See case 1a* t_1=19.8 EDY (nominal)	*See case 1a* t_1=20.8 EDY (nominal)
	2a	Load Module Bending Stress *Increase bending load per NB-3600 Eq.10*	*MNTEy*= 4519.4 MPa	M_{NTEy}=8585.4 MPa
	2b	Load Module Bending Stress *Increase bending load per NB-3600 Eq.10 with tref offset*	*See case 1a* t_1=19.8 EDY (nominal)	*See case 1a* t_1=9.0 EDY (nominal)
	3	Peening Penetration Depth *Double standard deviation of peening penetration depth*	$\sigma(x_{1,PPRS})$=0.25 mm	$\sigma(x_{1,PPRS})$=0.50 mm
	4	Stress Relaxation *Include time-dependent stress relaxation*	m=0.0 EFPY^{-1} $\sigma_{0,PPRS}(t=0)$=406 MPa (nominal)	m=5.1E-03 EFPY^{-1} $\sigma_{0,PPRS}(t=0)$=545 MPa (nominal)
	5	Multiple Flaw Initiation Model Slope *Increase to 3.0*	β_{flaw}=2.0	β_{flaw}=3.0
	6	Initiation-Growth Correlation *Include correlation*	ρ_{weld}=0.0 ρ_{ww}=0.0	ρ_{weld}=-0.8 ρ_{ww}=-0.8
	7	Stress Adjustment of Initiation Times *Remove*	n=4.0 (nominal)	n=0.0 (nominal)
	8	Initial Crack Depth *Decrease to 0.5% through-wall*	a_0/t=0.05 (nominal) 0.01 (lower bound) 0.42 (upper bound)	a_0/t=0.005 (nominal) 0.001 (lower bound) 0.42 (upper bound)
	9	Initiation Reference Time *Decrease reference time by factor of 5*	t_1=19.8 (nominal) 1.93 (lower bound) 202.7 (upper bound)	t_1=3.96 (nominal) 0.386 (lower bound) 40.5 (upper bound)
	10	Growth Integration Time Step *Halve*	1/12 yr	1/24 yr
	11	Initial Crack Depth and Minimum K Value *Decrease median initial crack depth to 0.5% through-wall* *Impose minimum K value of 12.0*	*See case 8* Minimum allowable K value= 0.0	*See case 8* Minimum allowable K value= 12.0
	12	Coalescence Threshold Distance *Increase threshold*	$F_{coalesce}$=1E06	$F_{coalesce}$=2.0
	13	Crack Closure Methodology *Utilize*	Neglected effect of crack closure on stress intensity factor	Accounted for effect of crack closure on stress intensity factor
	14	Balloon Growth *Prevent*	Neglected peening stresses for crack length growth	Accounted for peening stresses for crack length growth
	15	UT Inspection Correlation *Remove correlation between inspections*	ρ_{insp}=0.5	ρ_{insp}=0.0
	16	Axial Crack POD Reduction Factor *Decreased by 25%*	$f_{UT,axial}$=0.8	$f_{UT,axial}$=0.6
	17	Crack Detection *Disable detection of cracks less than 10% through-wall*	Linearly interpolated POD between 0 and 10% through-wall	Set POD to zero for cracks less than 10% through-wall
	18	Prior Plant Experience *Reject trials with detections/leaks before present day*	Did not apply rejection criterion	Rejected detections/leaks prior to 17 cycles of operation.

Table A-14
Description of Inspection Sensitivity Cases for DM Weld Probabilistic Model

Category	Case No.	Inspection Sensitivity Case		
		Parameter	***Base Case***	***New Value(s)***
Base	0	Base Case: *See table of base case inputs*		
Sensitivity	1	Inspection Scheduling *Skip follow-up inspection and enter ISI immediately*	Performed follow-up inspection one cycle after peening before entering ISI with inspection every interval	Skipped follow-up inspection before entering ISI with inspection every interval
	2	Inspection Scheduling *Skip UT during pre-peening inspection*	Performed UT during pre-peening inspection	Skipped pre-peening inspection
	3	Inspection Scheduling *Perform ET during pre-peening inspection*	Did not perform ET during pre-peening inspection	Performed ET during pre-peening inspection

Figure A-17
Prediction of Leakage vs. Time for RVON

Figure A-18
Prediction of Leakage vs. Time for Cold Leg RCP Inlet/Outlet Nozzle

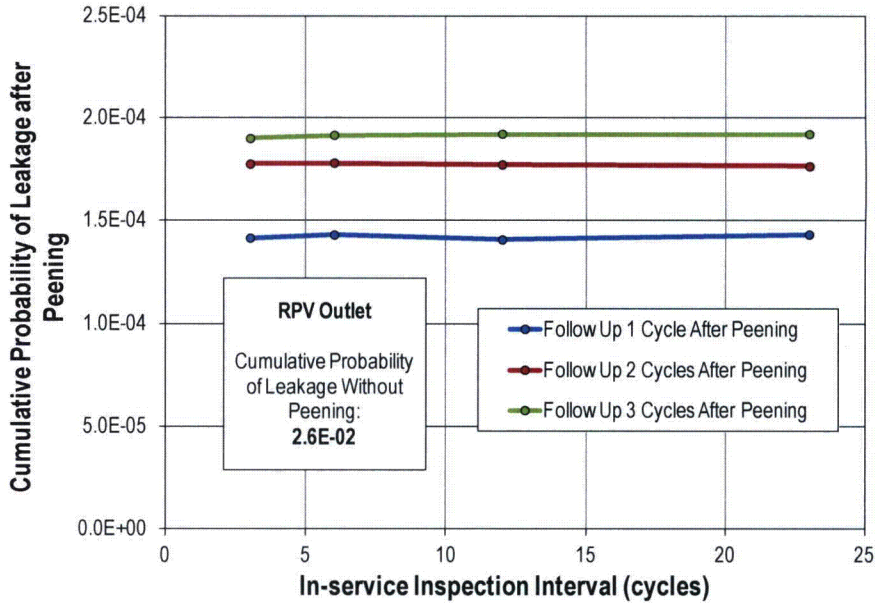

Figure A-19
Cumulative Probability of Leakage after Hypothetical Time of Peening vs. ISI Frequency for a RVON

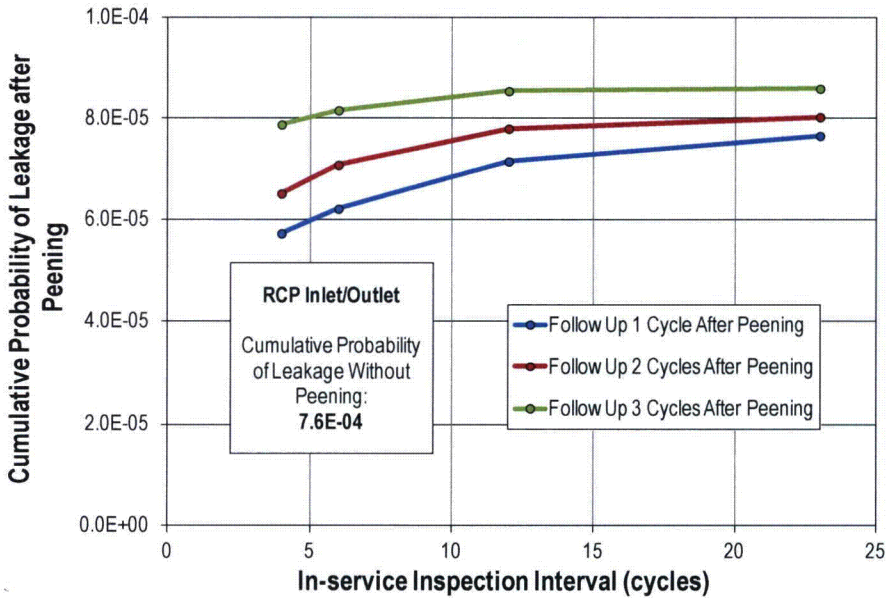

Figure A-20
Cumulative Probability of Leakage after Hypothetical Time of Peening vs. ISI Frequency for a Cold Leg RCP Inlet/Outlet Nozzle

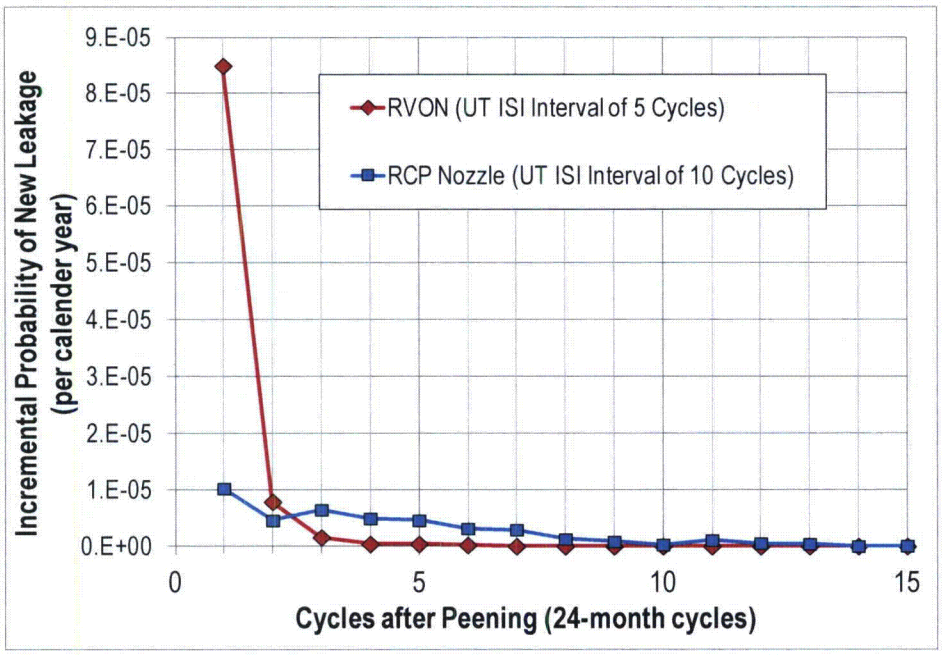

Figure A-21
Incremental Probability of Leakage after Peening with Relieved ISI Intervals (Follow-Up Inspection 1 Cycle After Peening)

Figure A-22
Summary of Sensitivity Results for DM Weld Probabilistic Model with Peening (RVON, Follow-Up Inspection 1 Cycle After Peening, ISI Interval of 6 Cycles)

Figure A-23
Summary of Sensitivity Results for DM Weld Probabilistic Model without Peening (RVON)

A.10 Conclusions regarding appropriate in-service examination requirements for DMWs in primary system piping mitigated by peening

The results of the probabilistic analysis of PWSCC on a general cold leg nozzle support the relieved UT inspection schedules prescribed in Section 4 of this report. Specifically, the cumulative leakage probability after the hypothetical time of peening is predicted to be reduced by:

- A factor of approximately 10 when the follow-up UT inspection is scheduled two cycles after peening and subsequent UT inspections are scheduled every 20 years (every two intervals)
- A factor of approximately 9 when the follow-up UT inspection is scheduled three cycles after peening and subsequent UT inspections are scheduled every 20 years (every two intervals)

The results of the probabilistic analysis of PWSCC on a general hot leg nozzle support the relieved UT inspection schedules prescribed in Section 4 of this report. Specifically, the cumulative leakage probability after the hypothetical time of peening is predicted to be reduced by:

- A factor of approximately 180 when the follow-up UT inspection is scheduled one cycle after peening and subsequent UT inspections are scheduled every 10 years (every interval)
- A factor of approximately 150 when the follow-up UT inspection is scheduled two cycles after peening and subsequent UT inspections are scheduled every 10 years (every interval)

For both hot and cold leg components, the probabilistic model predicts the rapid decay of incremental leakage probabilities after peening. Taking into consideration wastage concerns, the nature of this decay supports the relief of visual inspection scheduling approximately three cycles after peening.

Many key input or modeling assumptions have been varied for Model Sensitivity Cases. While the leakage probability predictions are shown to vary for many of these cases, no case negates the prediction that a peened hot leg component can maintain a lower probability of leakage with a relieved inspection schedule (as compared to the unmitigated component). This is due primary to the large margin of improvement predicted for the base case.

Three Inspection Sensitivity Cases investigate the impact of optional alterations to the inspection schedule/scope. Inspection Sensitivity Case 2 demonstrates the importance of a pre-peening UT inspection and Inspection Sensitivity Case 3 predicts a significant added value to a pre-peening ET inspection.

A.11 References

1. D. Rudland, et al., "Development of Computational Framework and Architecture for Extremely Low Probability of Rupture (xLPR) Code," *Proceedings of the ASME 2010 Pressure Vessels & Piping Division / K-PVP Conference: PVP2010*, Bellevue, Washington, July 2010.
2. *xLPR Pilot Study Report.* U.S. NRC-RES, Washington, DC, and EPRI, Palo Alto, CA: NUREG-2110 and EPRI 1022860. 2012.
3. W. H. Press, S. A. Teukolsky, W. T. Vetterling, B. P. Flannery, *Numerical Recipes. The Art of Scientific Computing. Third Edition.* Cambridge University Press, Cambridge, MA, 2007.
4. *Materials Reliability Program: Technical Basis for Primary Water Stress Corrosion Cracking Mitigation by Surface Stress Improvement (MRP-267, Revision 1)*, EPRI, Palo Alto, CA: 2012. 1025839.
5. *Materials Reliability Program Generic Evaluation of Examination Coverage Requirements for Reactor Pressure Vessel Head Penetration Nozzles, Revision 1 (MRP-95R1)*, EPRI, Palo Alto, CA: 2004. 1011225.
6. R. B. Abernethy, *The New Weibull Handbook, Second Edition*, Robert B. Abernethy, North Palm Beach, Florida, 1996.
7. *PWSCC Prediction Guidelines*, EPRI, Palo Alto, CA: 1994. TR-104030.
8. T. L. Anderson, et al., "Development of Stress Intensity Factor Solutions for Surface and Embedded Cracks in API 579," *Welding Research Council Bulletin 471*, May 2002.
9. S. Marie, et al., "French RSE-M and RCC-MR code appendices for flaw analysis: Presentation of the fracture parameters calculation – Part III: Cracked Pipes," *International Journal of Pressure Vessels and Piping*, 84, pp. 614-658, 2007.
10. S. Xu, et al., "Technical Basis for Proposed Weight Function Method for Calculation of Stress Intensity Factor for Surface Flaws in ASME Section XI Appendix A," *Proceedings of the ASME 2011 Pressure Vessels & Piping Division / K-PVP Conference: PVP2011*, Baltimore, Maryland, July 2011.
11. *3-D Finite Element Software for Cracks: User's Manual v2.7.* Structural Reliability Technology – FEA Crack.
12. *Materials Reliability Program: Technical Bases for the Chemical Mitigation of Primary Water Stress Corrosion Cracking in Pressurized Water Reactors (MRP-263)*, EPRI, Palo Alto, CA: 2009. 1019082.
13. *ASME Boiler and Pressure Vessel Code 2011, Section XI, IWA-3330*, ASME, 2011.
14. M. Beghini and L. Bertini, "Fatigue Crack Propagation Through Residual Stress Fields with Closure Phenomena," *Engineering Fracture Mechanics*, Vol. 36, No. 3, pp. 379-387, 1990.

15. D. Rudland, et al., "PWSCC Crack Growth Mitigation with Inlay," *Proceedings of the ASME 2011 Pressure Vessels & Piping Division Conference: PVP2011*, Baltimore, Maryland, July 2011.

16. Case N-770-1, "Alternative Examination Requirements and Acceptance Standards for Class 1 PWR Piping and Vessel Nozzle Butt Welds Fabricated With UNS N06082 or UNS W86182 Weld Filler Material With or Without Application of Listed Mitigation Activities," Section XI, Division 1, American Society of Mechanical Engineers, New York, Approval Date: December 25, 2009.

17. *Materials Reliability Program: Development of Probability of Detection Curves for Ultrasonic Examination of Dissimilar Metal Welds (MRP-262, Revision 1) – Typical PWR Leak-Before-Break Line Locations*, EPRI, Palo Alto, CA: 2009. 1020451.

18. *PWR Materials Reliability Project, Interim Alloy 600 Safety Assessments for US PWR Plants (MRP-44): Part 1: Alloy 82/182 Pipe Butt Welds*, EPRI, Palo Alto, CA,: 2001. TP-1001491, Part 1.

19. *Materials Reliability Program: Probabilistic Assessment of Chemical Mitigation of Primary Water Stress Corrosion Cracking in Nickel-Base Alloys (MRP-307), Zinc Addition and Hydrogen Optimization Mitigate Primary Water Stress Corrosion Cracking in Westinghouse Reactor Vessel Outlet Nozzles and Babcock & Wilcox Reactor Coolant Pump Nozzles*, EPRI, Palo Alto, CA: 2011. 1022852.

20. *Advanced FEA Evaluation of Growth of Postulated Circumferential PWSCC Flaws in Pressurizer Nozzle Dissimilar Metal Welds (MRP-216): Evaluations Specific to Nine Subject Plants*, EPRI, Palo Alto, CA: 2007. 1015383.

21. *Materials Reliability Program: Crack Growth Rates for Evaluating Primary Water Stress Corrosion Cracking (PWSCC) of Alloy 82, 182, and 132 Welds (MRP-115)*, EPRI, Palo Alto, CA: 2004. 1006696.

22. J. A. Gorman, et al., "Correlation of Temperature with Steam Generator Tube Corrosion Experience," *Fifth International Symposium on Environmental Degradation of Materials in Nuclear Power Systems – Water Reactors*, E. Simonen and D. Cubicciotti, eds., American Nuclear Society, LaGrange Park, Illinois, 1992.

23. *Statistical Analysis of Steam Generator Tube Degradation*, EPRI, Palo Alto, CA: 1991. NP-7493.

24. C. Amzallag, et al., "Stress Corrosion Life Assessment of Alloy 600 PWR Components," *Ninth International Symposium on Environmental Degradation of Materials in Nuclear Power Systems – Water Reactors*, Edited by F.P. Ford et al., The Minerals, Metals & Materials Society (TMS), 1999.

25. Outline of Hitachi-GE GE Nuclear Energy (HGNE)'s ECT and UT technologies for nickel based weld lines of BWR bottom head, Hitachi-GE document E-TY-50521r1, Feb. 1, 2012.

26. Eddy Current Examination Technique Specification Sheets (ETSSs) are available from the EPRI NDE Center, Charlotte, NC.

27. Y. Yi and G. S. Was, "Stress and Temperature Dependence of Creep in Alloy 600 in Primary Water," *Metallurgical and Materials Transactions A,* Vol. 32, No. 10, pp. 2553-2560, 2001.

28. *Companion Guide to the ASME Boiler and Pressure Vessel Code Vol. 1*, ASME, 2009.

29. M. Taniguchi and N. Hori, "Maintenance Technology Development for Alloy 600 PWSCC Issue," *Proceedings of ICONE12 12th International Conference on Nuclear Engineering*, April 25–29, 2004, Arlington, Virginia, USA.